

Early Eocene magnetostratigraphy and tectonic evolution of the Xining Basin, NE Tibet

Niels Meijer, Guillaume Dupont-Nivet, Alexis Licht, Pierrick Roperch, Alexander Rohrmann, Aijun Sun, Shengcheng Lu, Amber Woutersen, Norbert Nowaczyk

▶ **To cite this version:**

Niels Meijer, Guillaume Dupont-Nivet, Alexis Licht, Pierrick Roperch, Alexander Rohrmann, et al.. Early Eocene magnetostratigraphy and tectonic evolution of the Xining Basin, NE Tibet. Basin Research, 2023, 35 (2), pp.510-529. 10.1111/bre.12720 . hal-03805202

HAL Id: hal-03805202
https://hal.science/hal-03805202

Submitted on 7 Oct 2022

HAL is a multi-disciplinary open access archive for the deposit and dissemination of scientific research documents, whether they are published or not. The documents may come from teaching and research institutions in France or abroad, or from public or private research centers.

L'archive ouverte pluridisciplinaire **HAL**, est destinée au dépôt et à la diffusion de documents scientifiques de niveau recherche, publiés ou non, émanant des établissements d'enseignement et de recherche français ou étrangers, des laboratoires publics ou privés.



Distributed under a Creative Commons Attribution 4.0 International License

Meijer Niels (Orcid ID: 0000-0002-2186-5682)

Early Eocene magnetostratigraphy and tectonic evolution of the Xining Basin, NE Tibet

Niels Meijer[1*], Guillaume Dupont-Nivet[2], Alexis Licht[3], Pierrick Roperch[2], Alexander Rohrmann[4], Aijun Sun[5,6,7], Shengcheng Lu[8], Amber Woutersen[9], Norbert Nowaczyk[10]

1) Senckenberg Biodiversity and Climate Research Centre (SBiK-F), Senckenberganlage 25, D-60325 Frankfurt am Main, Germany.

2) Univ Rennes, CNRS, Géosciences Rennes - UMR CNRS 6118, F-35000 Rennes, France.

3) Aix Marseille University, CNRS, IRD, INRAE, CEREGE, Aix-en-Provence, France.

4) Institute of Geological Sciences, Freie Universität Berlin, Berlin, Germany.

5) Key Laboratory of Western China's Environmental Systems (Ministry of Education), College of Earth and Environmental Sciences, Lanzhou University, Lanzhou 730000, China.

6) Key Laboratory of Desert and Desertification, Northwest Institute of Eco-Environment and Resources, Chinese Academy of Sciences, Lanzhou 730000, China.

7) University of Chinese Academy of Sciences, Beijing 100049, China.

8) School of Urban Construction and Environment, Dongguan City College, Dongguan 523419, China.

9) Department of Ecosystem and Landscape Dynamics (ELD), Institute for Biodiversity and Ecosystem Dynamics (IBED), University of Amsterdam, Amsterdam 1090 GE, the Netherlands.

10) GFZ German Research Centre for Geosciences, Telegrafenberg, 14473 Potsdam, Germany.

*niels.meijer@senckenberg.de

Abstract

This article has been accepted for publication and undergone full peer review but has not been through the copyediting, typesetting, pagination and proofreading process which may lead to differences between this version and the Version of Record. Please cite this article as doi: 10.1111/bre.12720

This article is protected by copyright. All rights reserved.

Accepted Article

Accepted Article

The Cenozoic strata of the Xining Basin, NE Tibet, have provided crucial records for understanding the tectonic and paleo-environmental evolution of the region. Yet, the age for the lower part of the sedimentary stratigraphy and consequently the early tectonic evolution of the basin remain debated. Here, we present the litho- and magnetostratigraphy of various early Eocene sections throughout the Xining Basin independently constrained by the U-Pb radiometric age of a carbonate bed. Our study extends the dated stratigraphy down to 53.0 Ma (C24n.1r) and reveals highly variable accumulation rates during the early Eocene ranging from 0.5 to 8 cm/ka. This is in stark contrast to the low but stable accumulation rates (2-3 cm/ka) observed throughout the overlying Paleogene and Neogene strata. Such a pattern of basin infill is not characteristic for flexural subsidence as previously proposed, but rather supports an extensional origin of the Xining Basin with multiple depocenters, which subsequently coalesced into a more stable and slowly subsiding basin. Whether this extension was related to the far-field effects of the subducting Pacific Plate or the India-Asia collision remains to be confirmed by future studies.

Keywords: Xining Basin, geochronology, paleomagnetism, northeast Tibet, stratigraphy, Eocene.

1. Introduction

The Xining Basin, located on the northeastern margin of the Tibetan Plateau, has provided valuable Cenozoic sedimentary records which have been extensively studied for reconstructing the evolution of atmospheric moisture (Abels et al., 2011; Bosboom et al., 2014; Dupont-Nivet et al., 2007; Fang et al., 2015; 2019; Meijer et al., 2019; Yang R. et al., 2019), temperature (Page et al., 2019), vegetation (Dupont-Nivet et al., 2008a; Hoorn et al., 2012; Licht et al., 2020), dust fluxes (Licht et al., 2014; 2016; Meijer et al., 2021; Ruan et al., 2019) and the tectonic history of the region (Dai et al., 2006; Dupont-Nivet et al., 2004; 2008b; Fan et al., 2019; He et al., 2021; Horton et al., 2004; Yang R. et al., 2017; Yang F. et al., 2019;

Zhang et al., 2016). However, age models for the early evolution of the basin remain unclear because the Xiejia section, which is the longest and most continuous section in the basin and therefore often cited for the age model (Dai et al., 2006; Meijer et al., 2019; Yang F et al., 2019), is underlain by a fault and lacks the lowermost stratigraphy.

This has important implications for understanding the tectonic origin of the basin which has been argued to be formed by flexure (e.g. He et al., 2021; Liu et al., 2013), extensional normal faults (Fan et al., 2019) or transtension (Wang et al., 2013; 2016; Zhang et al., 2016). In turn, these tectonic processes may be related to the far-field effects of either the Pacific Plate subduction or the India-Asia collision and are therefore crucial for understanding the active tectonic drivers in the region. Especially because well-dated early Eocene deposits are rare in the northeastern Tibetan Plateau ever since the age model of the Qaidam Basin has been up for debate (e.g. Cheng et al., 2021) with one interpretation suggesting an early Eocene origin (e.g. Ji et al., 2017; Yin et al., 2008) and the other an Oligocene to Miocene time of formation (Nie et al., 2020; Wang et al., 2017). Therefore, improved age constraints and basin evolution reconstructions are needed to test the competing tectonic models in this region. Here, we present a basin-scale litho- and magnetostratigraphic study of the Xining Basin to reconstruct the early Eocene evolution of the basin. We constrain our age model with a radiometric age derived from a carbonate bed.

2. Geologic setting

The modern-day Xining Basin is located on the north-eastern margin of the Tibetan Plateau and is bounded by the Riyue Shan in the west, the Daban Shan (eastern Qilian Shan) in the north and the Laji Shan in the south (**Fig. 1 A**). During the Mesozoic, the basin was part of the Xining-Minhe Basin which stretched towards Lanzhou in the east and to Guide in the south (Horton et al., 2004). Mesozoic strata include Middle Jurassic mudrocks and sandstones interlayered with coal beds, which are exposed only in the center of the Xining Basin (**Fig. 1**

Accepted Article

B; QBGMR, 1985). These are unconformably overlain by the Early Cretaceous Hekou Group and the Late Cretaceous Minhe Formation with another unconformity separating the two units (**Fig. 1 C**). Both consist of red mudrocks, sandstones and conglomerates and are observed to coarsen towards the south (Horton et al., 2004; QBGMR, 1985).

During the Cenozoic, the Xining Basin formed the western part of the Longzhong Basin which extended towards the Liupan Shan in the east and the Western Qinling Shan in the south (Horton et al., 2004). Paleogene strata comprise the Xining Group and include red mudrocks, sandstones and gypsum beds of the Qijiachuan, Honggou, Mahalagou and Xiejia Formations (sensu Fang et al., 2019; **Fig. 1 C**). The boundary between the Cretaceous and Paleogene strata is reported as an angular unconformity in some locations and a disconformity in others (He et al., 2021; QBGMR, 1985). Detrital zircons indicate that the Paleogene sediments were derived from both the Qilian Shan in the north and the Western Qinling Shan in the south (He et al., 2021; Zhang et al., 2016). Subsequent Neogene deformation resulted in uplift of the Laji Shan, which segmented the Longzhong Basin into smaller sub-basins (Horton et al., 2004; Lease et al., 2011). Neogene transpression in the Xining Basin resulted in several basement-cored folds such as the Xiaoxia anticline which exposes the stratigraphy (**Fig. 1 B**; Zhang and Cunningham, 2013). Neogene strata comprise the Guide Group and include mudrocks, sandstones and conglomerates of the Chetougou, Guanjiashan and Mojiazhuang Formations (sensu Fang et al., 2019; **Fig. 1 C**). Locally, an additional Neogene conglomeratic succession, termed the Zhongba Formation, has been recognized in the foothills of the southeastern Xining Basin unconformably overlying the Paleogene strata (He et al., 2021).

Accepted Article

Accepted Article

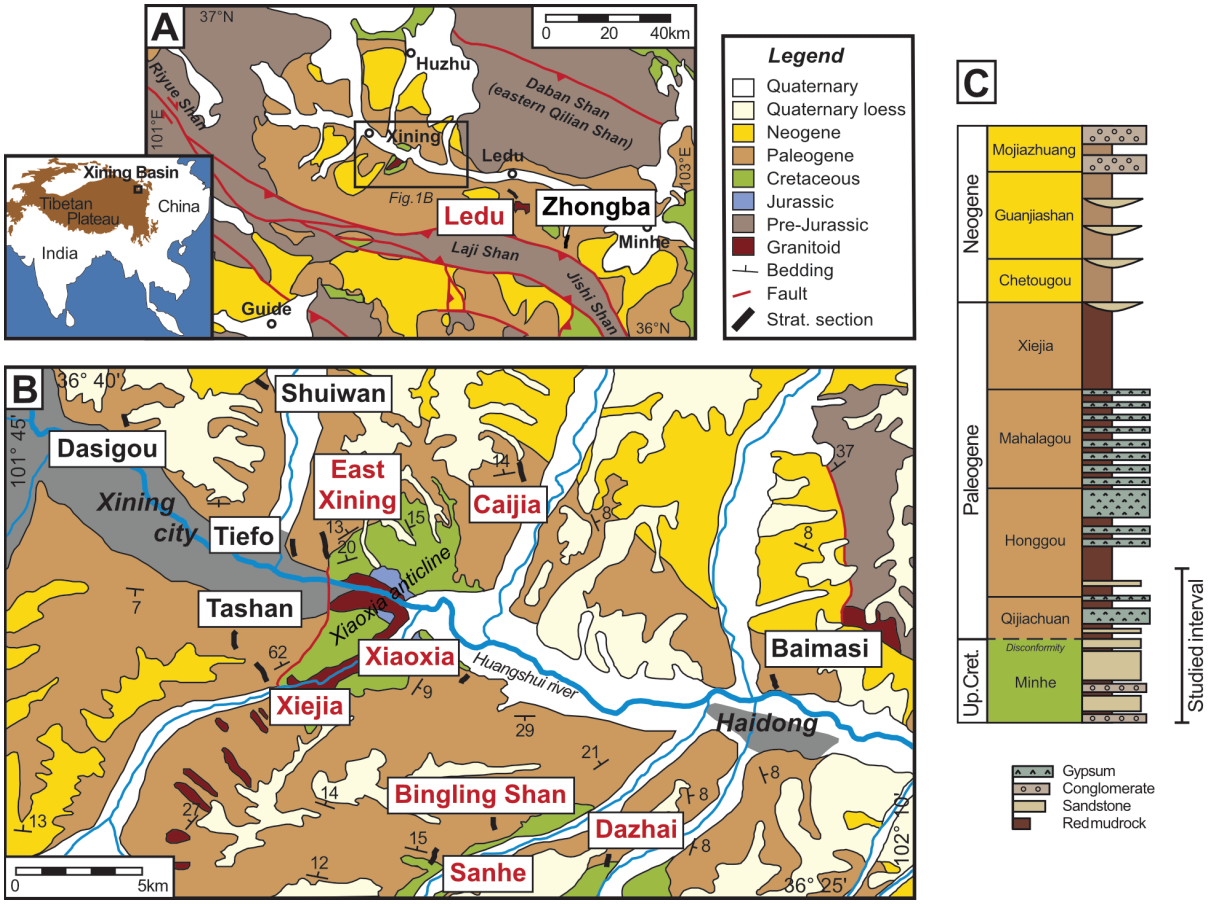


Fig. 1. A) Geological map of the Xining Basin (modified from Fan et al., 2019) showing the location of the studied Ledu section. Inset map shows the location of the Xining Basin. B) Detailed geological map (modified from BGMRQP, 1965 and QBGMR, 1985) showing the section locations near Xining city. Sections used in this study are indicated in red. C) Generalized lithostratigraphic column of the Xining Basin (based on QBGMR, 1985; Horton et al., 2004; Fang et al., 2019).

3. Methods

3.1 Sections and sampling

We studied the litho- and magnetostratigraphy of the Ledu section located in the eastern part of the Xining Basin (**Fig. 1 A**) and the following sections in the western part near Xining city (**Fig. 1 B**): Xiaoxia, Bingling Shan (lithostratigraphy previously studied by Dai et al., 2006),

Sanhe (lithostratigraphy previously studied by Zhang et al., 2016), and Dazhai (lithostratigraphy previously studied by Horton et al., 2004 and Zhang et al., 2016). We correlate these with the previously studied Xiejia, East Xining and Caijia sections (Meijer et al., 2019). Detailed GPS coordinates can be found in the Supporting Information. The lithostratigraphy was described in the field and paleomagnetic samples were collected at ~0.5 to 2 meter-resolution using an electric hand drill. The orientations of the paleomagnetic samples were measured using a compass mounted on an orientation stage. In addition, hand-sized rock samples were collected for rock magnetic analyses at Ledu and the previously studied Caijia section (Meijer et al., 2019) with a resolution of ~2 to 5 meters.

3.2 U-Pb dating of lacustrine carbonates

Fifteen lacustrine carbonates were collected throughout the sections for radiometric dating. The samples were cut to expose fresh surfaces and then incorporated into a 1-inch epoxy mount for in situ U-Pb dating. The mounts were then manually polished, first with coarse then fine (5 μm grit size) sandpaper. U-Pb dating was conducted by laser ablation inductively coupled plasma mass spectrometry (LA-ICP MS) at the TraceLab laboratory of the University of Washington. Hardware description, acquisition procedure, reference materials, and data reduction steps are described in Cong et al. (2021). Uncertainties are analytical and do not include the systematic uncertainty calculated from the long-term reproducibility of secondary reference materials, due to the current lack of international carbonate reference materials. The systematic uncertainty based on the long-term reproducibility of 10 zircon reference materials is ~2.67% (2σ) for $^{238}U/^{206}Pb$ ratios at the University of Washington (Licht et al., 2020).

3.3 Rock magnetism

The paleomagnetic samples of the Bingling Shan and Sanhe sections were analyzed at the Archeo-Paleomagnetic laboratory of Géosciences Rennes, France, the Dazhai section at the

Accepted Article

Accepted Article

Paleomagnetic Laboratory 'Fort Hoofddijk' of the Faculty of Geosciences at Utrecht University, the Netherlands, and the Ledu section at the Laboratory of Rock- and Paleomagnetism at the German Research Center for Geosciences (GFZ) in Potsdam. After measuring magnetic susceptibility, the samples were thermally demagnetized by stepwise heating up to 650°C using a MMTD48 in Rennes and an ASC Scientific TD48 in Utrecht and Potsdam. The Natural Remanent Magnetization (NRM) was measured after every step using a superconducting quantum interference device (SQUID). The magnetic susceptibilities of the samples were measured before the thermal demagnetization using a Bartington MS2 for the samples measured at Géosciences Rennes, and an AGICO Multifunction Kappabridge MFK-1A for the samples measured at the GFZ.

The hand samples of the Ledu and Caijia sections were carefully ground using a mortar and pestle and packed in cubic plastic boxes of 6 cm^3. Isothermal Remanent Magnetizations (IRM) were imparted using a 2G Enterprises 660 pulse magnetizer and subsequently measured using a Molspin spinner magnometer. The IRM intensity acquired at 1.5 T is defined here as the saturation IRM (SIRM) and, together with the IRM intensity acquired at a reversed field of 0.2 T, is used to define the S-ratio as: $0.5 \times (1 - [IRM_{-0.2T} / SIRM_{1.5T}])$. Detailed IRM acquisition curves were measured for selected samples using a 4" Princeton Measurements Corporation 'Micromag' alternating gradient magnometer (AGM). These S-ratios and IRM acquisition are used to characterize the magnetic components throughout the record.

4. Results

4.1 Lithostratigraphy and depositional environment

The lithostratigraphy of all sections is subdivided in formations and members following QBGMR (1985) and presented in **Fig. 2**. The East Xining, Xiejia and Caijia sections are from

Meijer et al. (2019). The lithofacies are described and the depositional environment is interpreted below.

Accepted Article

Accepted Article

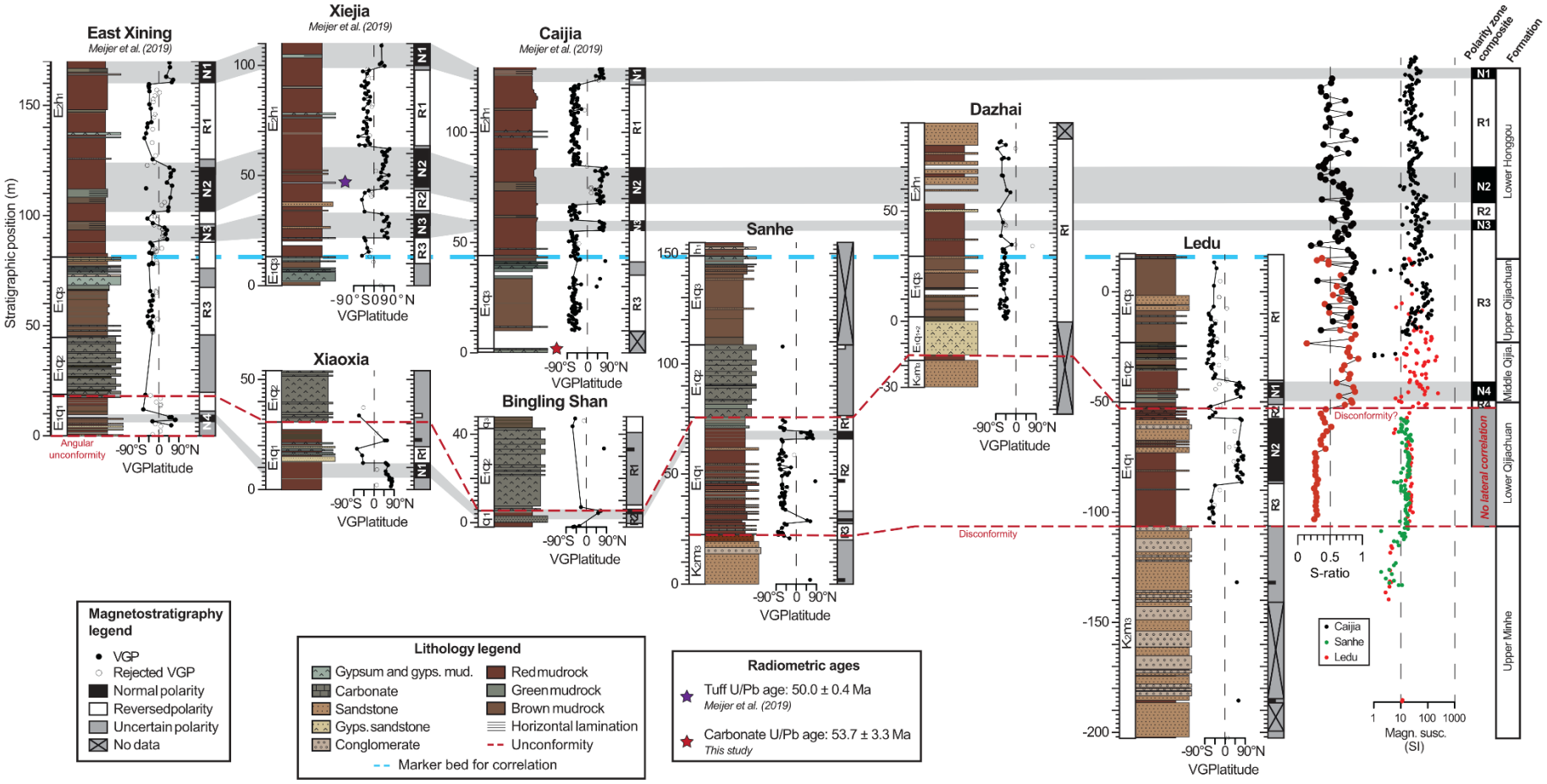


Fig. 2. Litho- and magnetostratigraphy of the studied sections. The East Xining, Xiejia and Caijia sections are from Meijer et al. (2019). The blue dashed line indicates the transition between the Qijiachuan and Honggou Formations which is used as a marker bed for correlating the sections. Rock magnetic properties are shown on the right as well as a composite of the polarity zones which are correlated to the geomagnetic polarity timescale in Fig. 8.

4.1.1 Upper Minhe Formation (K_2m^3)

Description

The upper Minhe Formation consists of dm- to m-scale beds of sandstone and conglomerate (**Fig. 3 A-D**). Some m-scale channels are observed in the sandstones. The conglomerates are both clast- and matrix-supported and are composed of poorly sorted, subangular to subrounded polymictic pebbles (**Fig. 3 D**). The sandstones are medium- to coarse-grained and poorly sorted containing subrounded granules and pebbles. The sedimentary structure is predominantly massive, but trough cross-bedding and horizontal bedding are observed occasionally as well (**Fig. 3 C**). The sandstones and conglomerates are interbedded with rare dm-scale beds of massive red mudrocks. These mudrocks become more abundant towards the north (**Fig. 3 E**).

Interpretation

The matrix-supported conglomerates in the upper Minhe Formation are interpreted as debris flow deposits and the clast-supported conglomerates and sandstones as braided river channel-fills (Smoot and Lowenstein, 1991). Consequently, the depositional environment of the upper Minhe Formation is interpreted as a proximal alluvial fan. The sediments are likely transported from the south as the upper Minhe Formation is fining towards the north (QBGMR, 1985).

Accepted Article

Accepted Article

4.1.2 Lower Qijiachuan Formation (E_1q^1)

Description

The Minhe Formation is overlain by the Qijiachuan Formation. At most locations this boundary is represented by a disconformity (**Fig. 3 A and B**) which may span ~20 Ma according to the magnetostratigraphy in the eastern Xinin Basin (He et al., 2021). An angular unconformity is observed at the East Xining section (**Fig. 3 E**). The lithofacies of the lower Qijiachuan Formation consist predominantly of massive red mudrocks containing slickensides due to swelling clays. In the western sections, these mudrocks occasionally contain cm- to dm-scale horizons of mottling (**Fig. 3 F**) in red (2.5YR 4/4), purplish (7.5R 4/3), yellow (2.5Y 5/4), grey (10GY 5/1) and dark grey (10B 3/1). The mudrocks are commonly interbedded with laterally extensive dm- to m-scale sandstone beds. These sandstones are medium- to coarse-grained, contain granules and have a massive, horizontally bedded or trough cross-bedded structure. Occasionally, the mudrocks and sandstones are interbedded with cm-scale micritic carbonate beds containing a horizontally laminated or massive structure.

Interpretation

The fine-grained deposits in the lower Qijiachuan Formation indicate low energy suspension settling and we interpret the depositional environment as a distal alluvial mudflat (Abels et al., 2011; Dupont-Nivet et al., 2007; Smoot and Lowenstein, 1991; Talbot et al., 1994). The mottled horizons and slickensides suggest that some of the mudrocks have been subjected to pedogenesis. The sandstones are interpreted as unconfined fluvial flows based on their lateral extent (North and Davidson, 2012). The carbonates may have formed in a lacustrine setting resulting in horizontal laminations or due to spring water as they are often observed to overlie the more porous sandstone beds (Smoot and Lowenstein, 1991).

4.1.3 Middle Qijiachuan Formation (E_1q^2)

Accepted Article

Description

The middle Qijiachuan Formation is characterized by a ~30 meters-thick package of organic-rich gypsum beds in the western part of the Xining Basin (**Fig. 3 A and G**) and previously described in Meijer et al. (2019). These beds have a massive to nodular structure and alternate on a dm-scale between light grey and darker grey beds due to a varying content in gypsum and organic material (~0.1-1.7%). The top ~2 meters of this package consists of horizontally laminated gypsum interbedded with cm-scale micritic carbonates. Towards the east, the lithofacies of the middle Qijiachuan Formation vary considerably. At the Dazhai section, the lithofacies consists of ~15 meters gypsiferous, medium-grained sandstone with a massive structure (**Fig. 3 B**). This is overlain by ~3 meters of organic-rich gypsiferous mudrocks. The gypsiferous sandstone is a local feature and the organic-rich gypsum package reappears, but is observed to thin towards the east. At the Ledu section, located ~30 km further towards the east, these characteristic gypsum beds are lacking completely. Instead, the lithofacies consist of red and grey massive mudrocks alternated with meter-scale intervals of dark grey, horizontally laminated mudrocks with a relatively high organic content (0.4%) and interbedded with cm-scale beds of nodular gypsum and micritic carbonate.

Interpretation

Based on the abundance of evaporites, we interpret the depositional environment of the middle Qijiachuan in the western part of the Xining Basin as a saline lake with the varying TOC reflecting fluctuations in salinity and/or productivity (Meijer et al., 2019). The abundance of sandstones at the Dazhai section indicates local fluvial deposition. The massive mudrocks at the Ledu section are interpreted as a distal alluvial mudflat alternated with intervals of lacustrine deposition as indicated by the horizontally laminated mudrocks (Abels et al., 2011; Dupont-Nivet et al., 2007; Meijer et al., 2019; Smoot and Lowenstein, 1991).

4.1.4 Upper Qijiachuan Formation (E_1q^3)

Accepted Article

Description

The boundary to the upper Qijiachuan Formation can be identified by a shift to mudrocks with a characteristic dark reddish brown color (**Fig. 3 A, B and H**), termed liver-brown in QBGMR (1985) and occurring throughout the basin. The mudrocks are massive and contain slickensides, rare carbonate nodules and are interbedded with cm-scale cross-laminated siltstones and dm-scale cross-bedded sandstones. The mudrocks have a relatively high organic content varying between 0.2-0.6%. In the western part of the basin, the top of the upper Qijiachuan Formation is characterized by dm-scale massive gypsum beds and green mudrocks alternated with cm-scale micritic carbonate beds (**Fig. 3 H**).

Interpretation

The depositional environment is interpreted as an organic-rich distal alluvial mudflat (Meijer et al., 2019). The organic material results in the liver-brown color of the mudrocks. The slickensides and carbonate nodules indicate subaerial exposure and pedogenesis. The silt- and sandstones indicate episodic fluvial activity by unconfined flows (North and Davidson, 2012). The top of the formation is interpreted as lacustrine deposits in a saline to alkaline environment (Meijer et al., 2019).

4.1.5 Lower Honggou Formation (E_2h^1)

Description

The transition to the lower Honggou Formation is marked by a shift to brick-red colored mudrocks with a massive structure (**Fig. 3 A, B and H**). This distinct shift can be recognized throughout the basin and is used as a marker bed to correlate the sections (blue dashed line in **Fig. 2**). The Honggou Formation has been described previously in Meijer et al. (2019) and will be summarized here. The red mudrocks are interbedded with m-scale intervals of brown-colored, horizontally laminated mudrocks, cm-scale carbonate beds and occasional dm-scale sandstone and gypsum beds. At the Dazhai section, we observe abundant dm- to m-scale

sandstone beds, which are laterally extensive, medium- to coarse-grained and have a massive or trough cross-bedded structure.

Interpretation

The depositional environment of the red mudrocks is interpreted as an alluvial mudflat alternated with alkaline to saline lacustrine conditions and occasional fluvial deposits (Meijer et al., 2019). The Dazhai section is interpreted as a more proximal setting as evidenced by the more abundant fluvial sandstones.

Accepted Article

Accepted Article

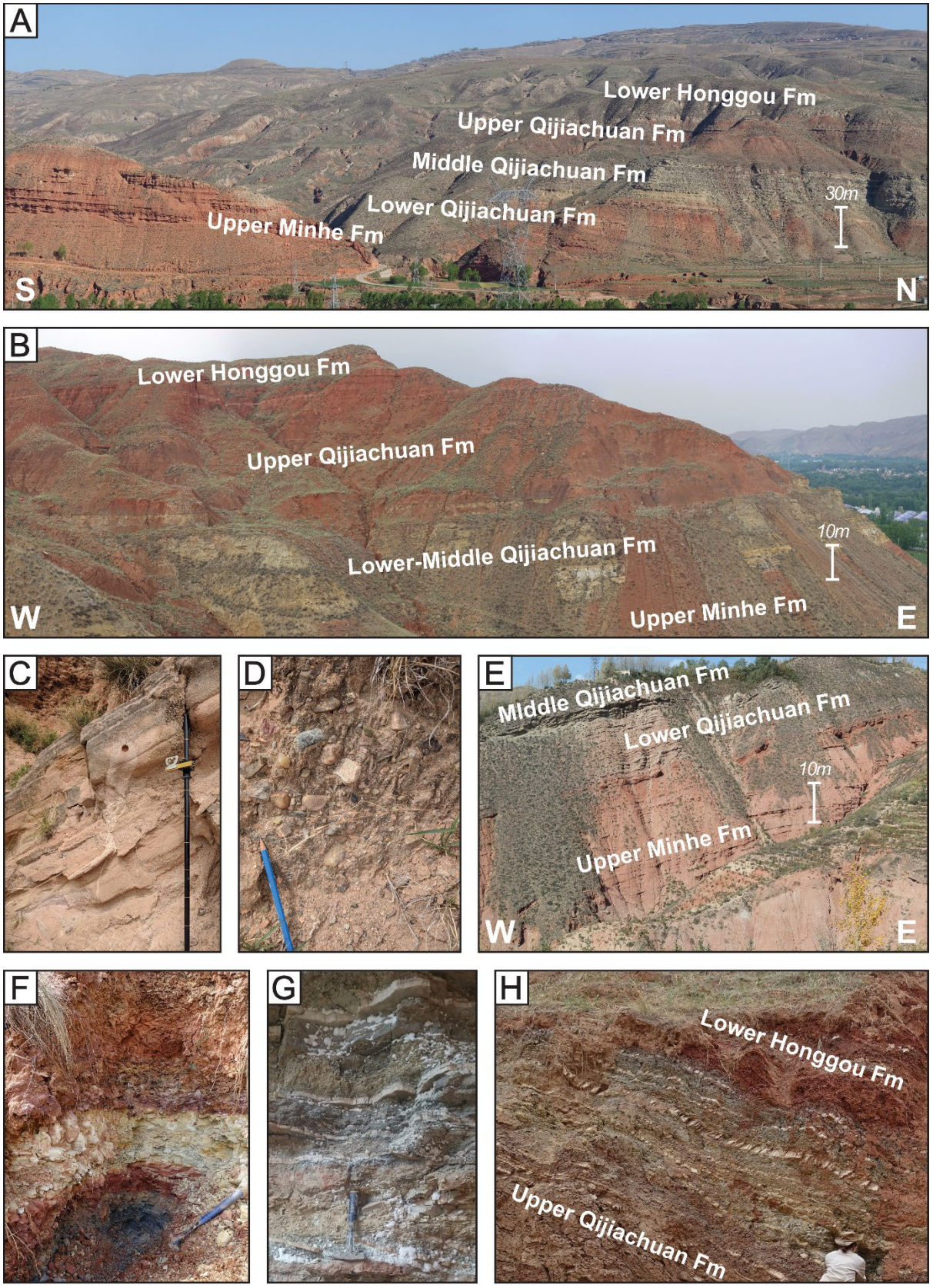


Fig. 3. Pictures of the studied sections and lithofacies. A) Overview of the Sanhe section. B) Overview of the Dazhai section. C) Sandstone of the Minhe Formation at the -150 meter-level

of the Ledu section. Jacob's staff with 10 cm-spaced markings for scale. D). Conglomerate of the Minhe Formation at the Ledu section showing the polymictic composition of the clasts. Pencil for scale. E) Overview of the base of the East Xining section showing an angular unconformity between the Minhe and Qijiachuan Formations. F) Yellow-white siltstone and variegated mudrocks at the 47-meter level of the Sanhe section. Hammer for scale. G) The middle Qijiachuan Formation at Bingling Shan showing alternations between light gray and darker gray gypsiferous mudrocks and gypsum beds. Secondary gypsum forms the white powdery coatings and fracture-filling fibrous gypsum forms the horizontal veins. Hammer for scale. H) Top of the Qijiachuan Formation at the Xiejia section showing liver-brown and green mudrocks interbedded with cm-scale carbonate beds and the transition to the brick-red mudrocks of the Honggou Formation. Person for scale.

4.2 Radiometric dating and magnetostratigraphy

4.2.1 U-Pb radiometric age

Meijer et al. (2019) radiometrically dated a tuff layer in the Honggou Formation at the Xiejia section, which constrained the age to 50.0 ± 0.4 Ma (**Fig. 2**). Here, we provide an additional radiometric age of a carbonate bed, CJC07, located at the top of the middle Qijiachuan Formation in the Caijia section (1.3 meter-level; **Fig. 2**). This was the only sample out of the fifteen that were measured that contained enough Uranium. The age was determined from the lower intercept on the Tera-Wasserburg plot (**Fig. 4**). The resulting age is 53.7 ± 3.3 Ma (2σ; MSWD: 0.4).

Accepted Article

Accepted Article

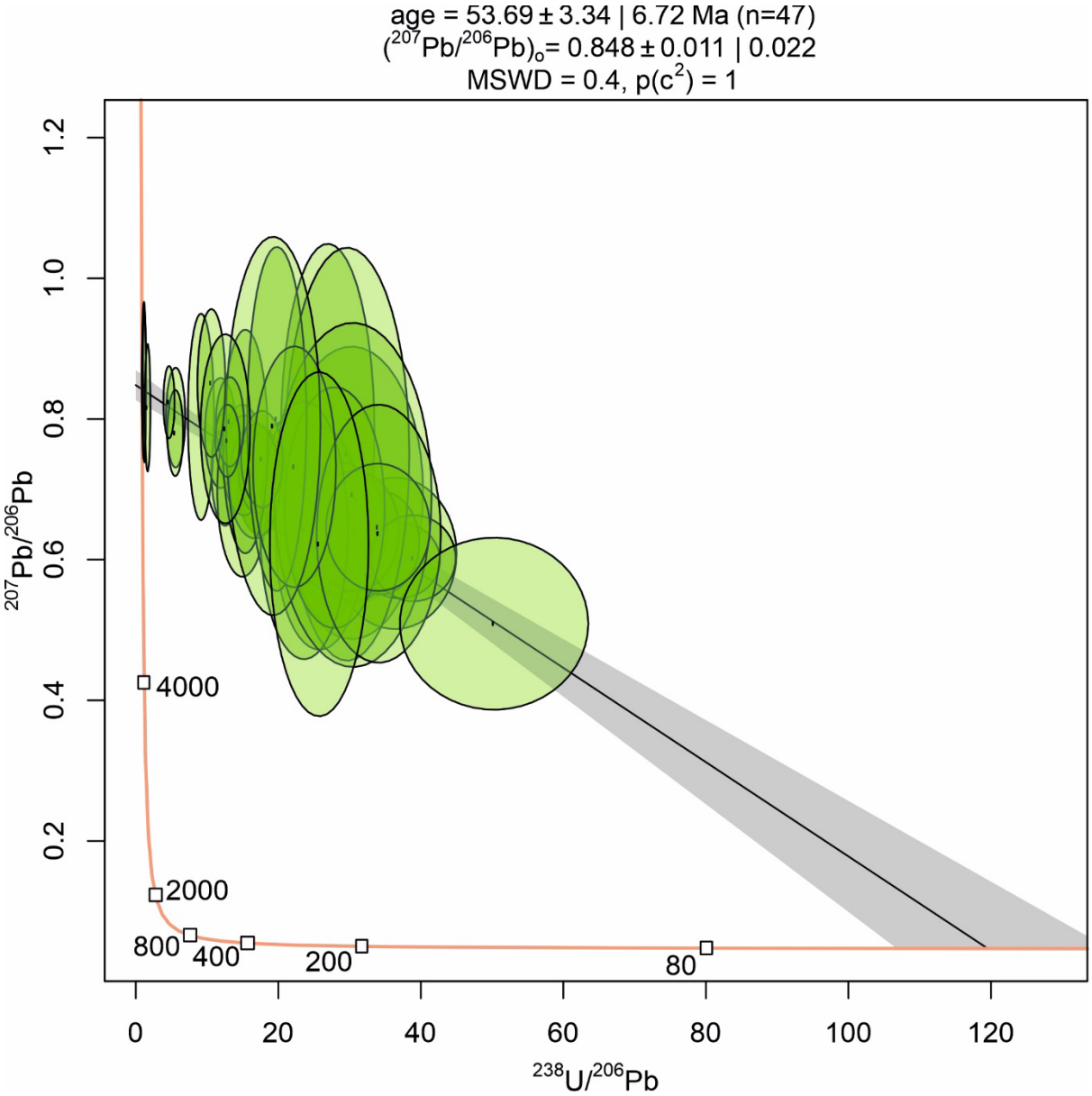


Fig. 4. Tera-Wasserburg diagram of the lacustrine carbonate sample CJC07.

4.2.2 Rock magnetism

The mudrocks sampled for magnetostratigraphy show an abrupt shift in rock magnetic properties occurring at the transition between the lower and middle Qijiachuan Formation. This shift is obscured in the western sections due to the low magnetic signal of evaporites in the middle Qijiachuan Formation, but can be clearly identified in the mudrocks of the Ledu section. Magnetic susceptibilities increase abruptly from ~20 × 10^{-5} to up to ~200 × 10^{-5} SI, while S-

ratios increase to mostly >0.5 (**Fig. 2**) and NRM increases to >10^{-3} A/m (**Fig. S1**). Magnetic susceptibilities remain relatively high throughout the upper Qijiachuan Formation and gradually decrease down to ~20 × 10^{-5} SI in the Honggou Formation.

Thermal demagnetization resulted in the removal of a viscous normal overprint up to ~200 °C (**Fig. 5**). High-susceptibility samples show a drop in NRM at ~580 °C indicating that magnetite is the main magnetic carrier. Samples with both high and low magnetic susceptibilities require temperatures beyond 650°C to completely demagnetize, which indicates the ubiquitous presence of hematite throughout the record. The abrupt transition observed in the S-ratios and magnetic susceptibilities of the Qijiachuan Formation thus represents a shift from hematite to magnetite as the dominant magnetic carrier. This is further supported by the IRM and hysteresis plots which show wasp-waisted loops due to a combination of different coercivities (e.g. Roberts et al., 1995) which can be unmixed in a soft component of magnetite and a hard component representing hematite (**Fig. 6** and **S2-S3**). In samples with a significant fraction of magnetite, the hysteresis parameters Bcr/Bc and Mrs/Ms are in the range (1.9-2.2) and (0.24-0.3) respectively, suggesting fine-grained single to pseudo-single domain magnetite. The low Bc value in hematite samples suggests that the hematite is very fine grained. Sandstones, conglomerates and gypsum beds do not preserve a stable remanent magnetization. This hampers reconstructing the magnetostratigraphy of the middle Qijiachuan Formation in the western part of the Xining Basin and the Minhe Formation.

Accepted Article

Accepted Article

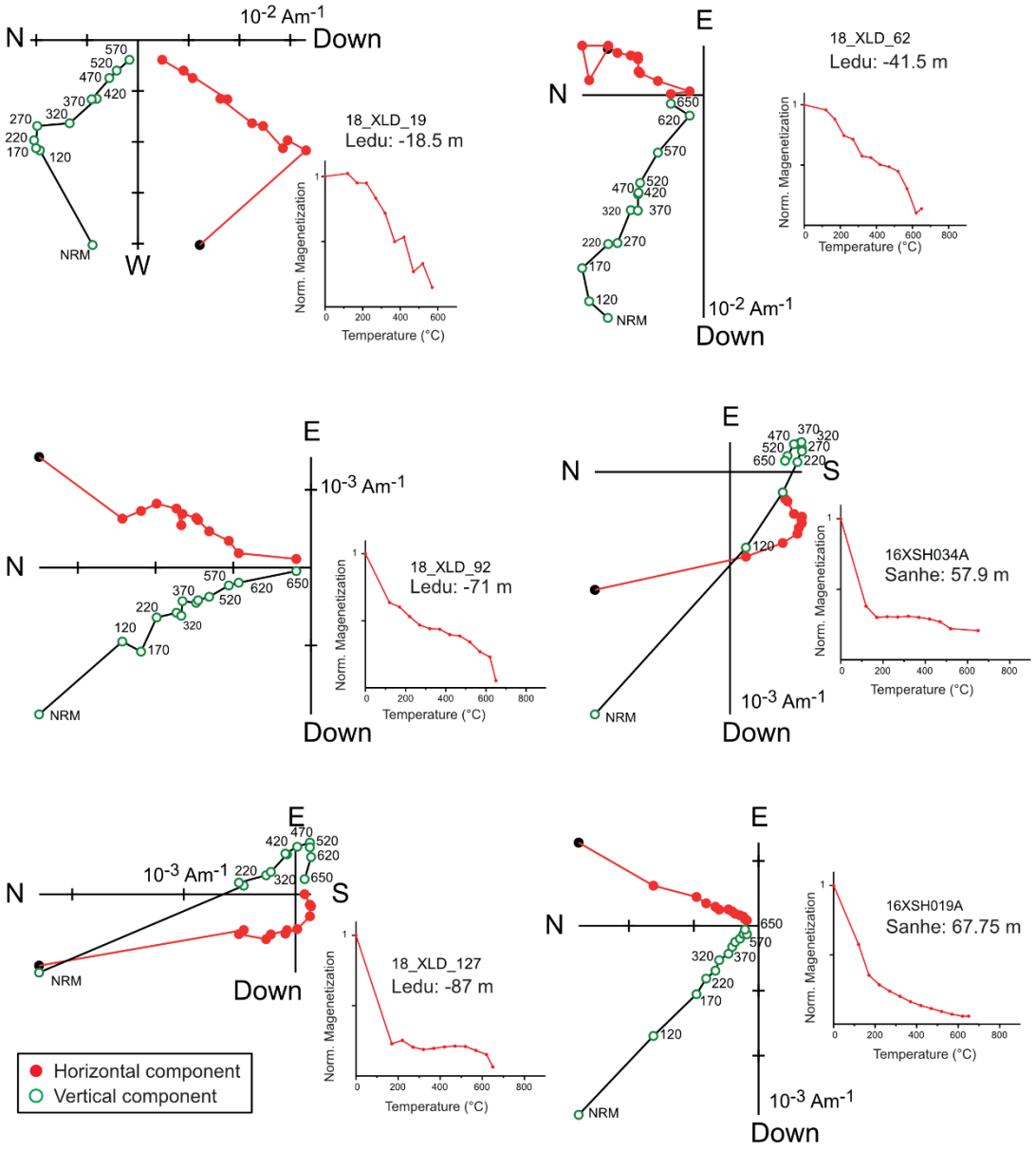


Fig. 5. Orthogonal plots of thermal demagnetization for six representative samples of the Ledu and Sanhe sections. Numbers indicate temperature steps in °C. Samples 18XLD19 and 18XLD62 from the Ledu section have magnetite as the main magnetic carrier, while the other

ChRMs and are shown in **Fig. 2**. Polarity zones are defined by at least two samples of the same polarity.

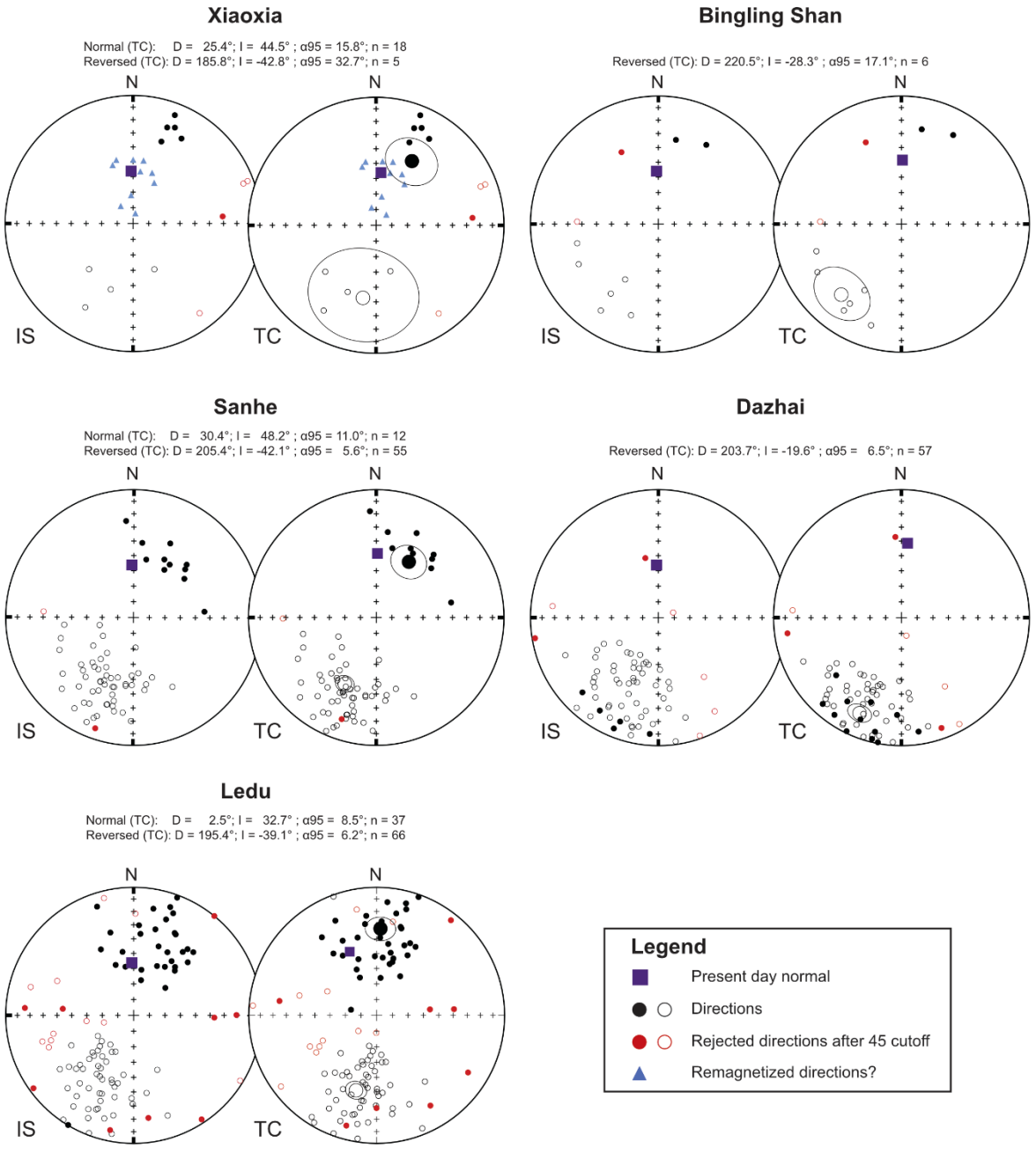


Fig. 7. Equal-area stereographic projections of calculated ChRM directions of the studied sections both in situ (IS) and tilt corrected (TC).

Accepted Article

samples are dominated by hematite. The coordinates of the plots are in situ.

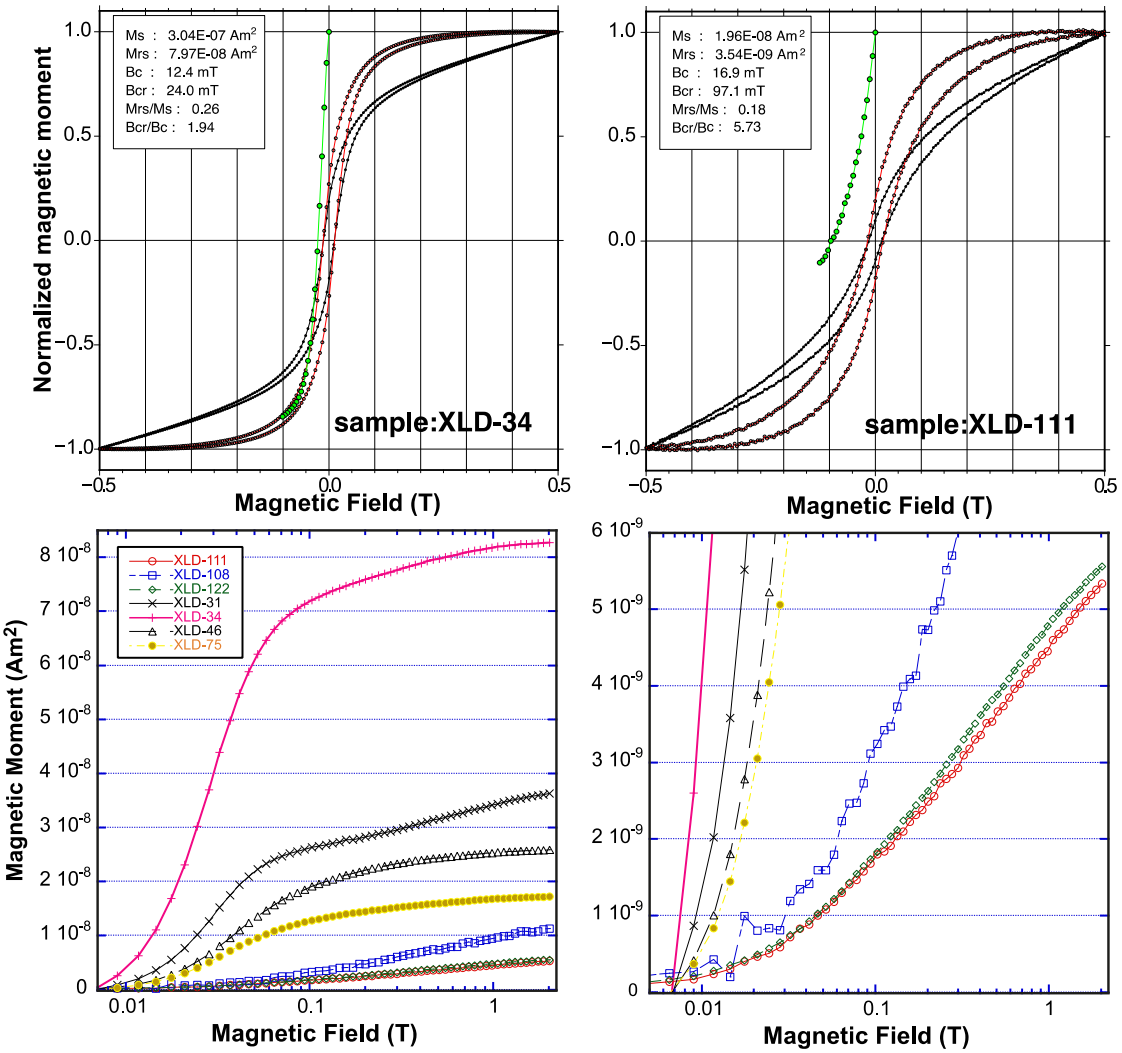


Fig. 6. High-field magnetic properties. Top) examples of hysteresis plots (black lines) for two samples of the Ledu section with magnetite (left) and hematite (right) as the dominant magnetic carrier, both showing a wasp-waisted loop. Red lines show the paramagnetic correction and green lines show the remanent curve. Bottom) IRM acquisition for seven samples of the Ledu section. The plot on the right is a zoom to highlight the low amount of magnetization acquired below 0.1 T in samples at the base of the Ledu section (XLD-108, XLD-111, XLD-122).

Accepted Article

Accepted Article

4.2.3 ChRM directions

Characteristic Remanent Magnetization (ChRM) directions were calculated for each sample using eigenvector principal component analysis on at least four temperature steps showing a linear decay between ~300-650 °C (**Fig. 5**; Kirschvink, 1980). Similar polarities and directions were observed in both the lower temperature magnetite and the higher temperature hematite components of each sample as also reported by Dai et al. (2006). The ChRMs were anchored to the origin and the directions resulting in a Maximum Angular Deviation (MAD) of >30° were rejected. However, most samples have a MAD of <10°.

The ChRMs show two clusters with either normal or reversed directions (**Fig. 7**). Mean directions were calculated using Fisher statistics (Fisher, 1953) and directions with an angle of more than 45° from the mean were rejected from further analysis (open symbols in **Fig. 2** and red symbols in **Fig. 7**). We performed a reversals test (McFadden and McElhinny, 1990) on the mean directions of the sections to check the reliability of our dataset. The test succeeded for the Sanhe section with classification C, but is indeterminate for the Xiaoxia section and failed for the Ledu and Bingling Shan sections. The poor performance of the reversals tests is due to an unresolved normal overprint which has been observed in previous magnetostratigraphic studies in the Xining Basin (Dupont-Nivet et al., 2008b; Meijer et al., 2019). This would exclude our dataset for the analysis of tectonic rotations, but does not affect the reliability of the reversals used in our magnetostratigraphy. Only in the Xiaoxia section we observe a cluster of normal directions similar to the modern-day field, suggesting that these may have been completely remagnetized (blue symbols in **Fig. 7**). These samples are from a weathered interval at the base of the section and are not considered as a polarity zone in the magnetostratigraphy (**Fig. 2**). Virtual Geomagnetic Poles (VGPs) were calculated from the

Accepted Article

4.2.4 Correlations to the geomagnetic polarity timescale

In the following, we first correlate the polarity zones between the different sections to create a composite (**Fig. 2**) and then correlate this to the geomagnetic polarity timescale (**Fig. 8**). We use the two astronomically tuned timescales that are currently available, the GTS20 (Ogg et al., 2020) and W2020 (Westerhold et al., 2020), but note that there are only minor differences of less than 300 ka between the two (**Fig. 8**).

The lower Honggou Formation contains three normal polarity zones (N1-N3 in the composite) which correlate well between the East Xining, Xiejia and Caijia sections (Meijer et al., 2019). Below is a long reversed polarity zone of up to 80 meters (R3 in the composite). This zone correlates well between the Qijiachuan liver-colored mudrocks of the East Xining, Caijia, Dazhai and Ledu sections. However, this zone is especially thick in the Dazhai section (R1) where it extends far into the overlying Honggou Formation. This interval contains abundant fluvial sandstones which may indicate locally higher accumulation rates and therefore a thicker reversed zone compared to the other sections. The lower part of composite R3 is only recorded at the Ledu section (R1), where it is underlain by an 8 meters-thick normal zone at the base of the middle Qijiachuan Formation (N1 in the Ledu section, N4 in the composite). The polarity zones in the lower Qijiachuan Formation are laterally inconsistent. At Ledu, this interval is characterized by a long normal zone bounded by reversed zones. But at Sanhe, this interval is mostly reversed with only two short normal polarity zones. The upper of these correlates with the East Xining, Xiaoxia and Bingling Shan sections, but not with the Ledu section. This may indicate more lateral variations in accumulation rates or gaps in the stratigraphic record because we note that the discrepancies between the polarity zones occur below the shift in rock magnetic properties. This shift may therefore mark an unconformity and will be discussed in more detail below.

Accepted Article

The magnetostratigraphy above can be extended up into the Neogene (Abels et al., 2011; Bosboom et al., 2014; Dai et al., 2006; Dupont-Nivet et al., 2007; Meijer et al., 2019; Xiao et al., 2012; Yang et al., 2017; 2019). Following these studies, N1 and N2 have been correlated to C21n and C22n respectively, which is further constrained by the radiometric age of a tuff layer in the Xiejia section (**Fig. 8**; Meijer et al., 2019). N3 can then be correlated to C23n (following Yang F. et al., 2019) and N4 to C24n.1n (preferred correlation in **Fig. 8**). This correlation would put the dated carbonate at 52.5 Ma and therefore well within the radiometric age constraints of 53.7 ± 3.3 Ma. However, polarity zone N3 does not fit the expected pattern of C23n and this correlation results in highly variable accumulation rates ranging from 0.5 cm/ka in C23n to 7 cm/ka in C23r (**Fig. 9**). Hence alternatively, N3 was interpreted as remagnetized and R2 and R3 have been correlated to C22r by Meijer et al. (2019), while N4 could be correlated to C23n.1n (rejected correlation in **Fig. 8**). This correlation would put the dated carbonate at 50.6 Ma and therefore also within the radiometric age constraints. However, it requires N3 to be ignored even though there is no evidence for remagnetization in both the lithologies and rock magnetic properties (Meijer et al., 2019). The intensity of the magnetization, unblocking temperatures and even the previously reported transformation of the magnetic minerals during heating at 500°C (Bosboom et al., 2014) are observed in both normal and reverse polarities (**Fig. S4**). Therefore, we do not observe remagnetization in these deposits except for the viscous overprint in the present-day field. Both correlations imply that accumulation rates are variable (**Fig. 9**), but we consider our preferred correlation to be the most parsimonious because it implies no additional normal chrons.

Our preferred correlation results in an age of 53.0 Ma (C24n.1r) at the base of the middle Qijiachuan Formation. We note that the underlying magnetostratigraphic pattern at the Ledu section (N2) fits well with the expected pattern of C24n.3n, while the short normal zones at Sanhe (N1 and N2) fit with the expected pattern of C25n and C26n. However, due to the lateral inconsistency between the polarity zones at the Sanhe and Ledu sections and the lack of additional age constraints, we refrain from further interpreting these polarity zones.

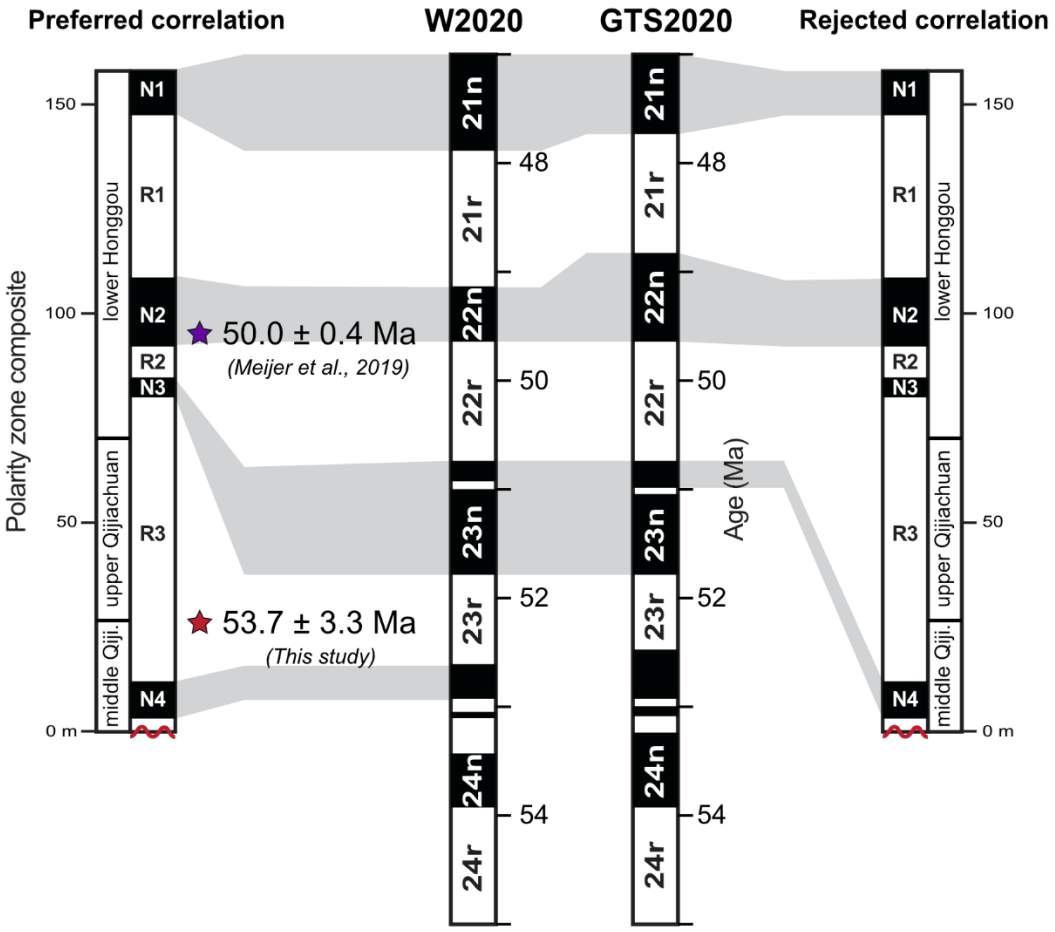


Fig. 8. Magnetostratigraphic correlations to the astronomically tuned geomagnetic polarity timescales of W2021 (Westerhold et al., 2021) and GTS2020 (Ogg et al., 2020). Polarity zones represent a composite of the sections shown in Fig. 2. Note that the overlying magnetostratigraphy of the Xining Basin extends up to the Neogene.

Accepted Article

Accepted Article

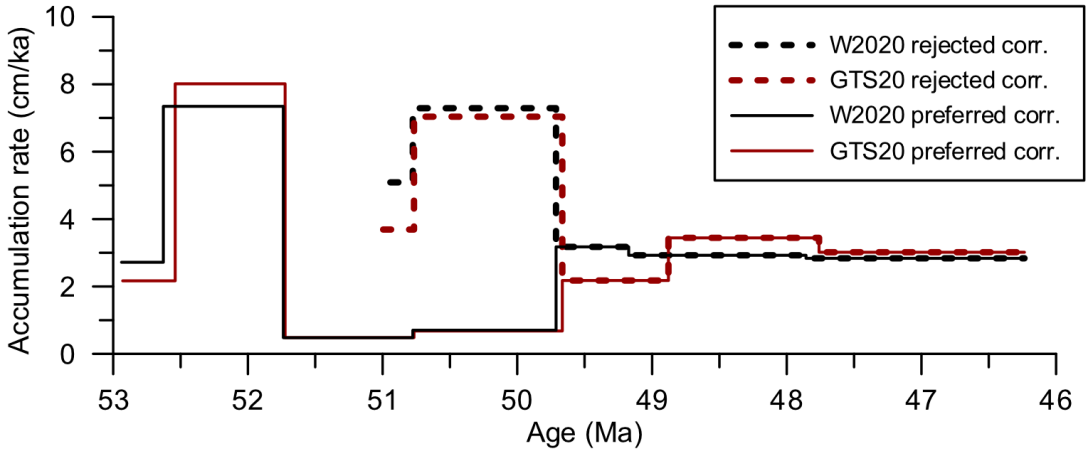


Fig. 9. Accumulation rates using the magnetostratigraphic correlations presented in this study and two astronomically tuned age models for the chron boundary ages (Gradstein et al., 2020 and Westerhold et al., 2020). Thicknesses of the polarity zones are derived from adding together the Ledu to the Caijia section at the Qijiachuan-Honggou transition (blue line in Fig. 2).

5. Discussion

5.1 Age model and basin infill

Our study extends the age model of the Xining Basin strata down to the early Eocene at 53.0 Ma. This age is older than the 49.3 Ma recorded at the Zhongba section in the eastern Xining Basin (He et al., 2021), but a more detailed comparison with this section is hampered by a lack of lithostratigraphic correlations. We also refine the age models of Dai et al. (2006) and Yang F et al. (2019) who interpreted the top of the Qijiachuan Formation as 53 Ma due to a viscous normal overprint recorded in the gypsiferous mudrocks at the base of the Xiejia section. In our magnetostratigraphy, the entire upper Qijiachuan Formation is reversed and the base of the Xiejia section corresponds to 52.0 Ma instead.

Accepted Article

We observe an abrupt shift from a hematite- to magnetite-dominated magnetic assemblage at the base of the middle Qijiachuan Formation. In the following, we discuss possible mechanisms for the appearance of this magnetite. As described above, we observe no evidence for remagnetization in these strata, except for the viscous normal overprint. This suggests that both magnetite and hematite have a detrital or early chemical origin soon after deposition. The transition to magnetite as the main magnetic carrier could thus represent a shift in provenance increasing the supply of detrital magnetite. A similar shift has been recognized in the Miocene strata of the Xining Basin where an increase in detrital magnetite was derived from plutonic and volcanic rocks from the uplifting Laji Shan and was coupled to unstable sedimentation rates and an unconformity (Xiao et al., 2012). Another increase in single domain magnetite was observed at 51.7 Ma in the neighboring Linxia Basin coeval with a shift in detrital zircons and linked to uplift of the Western Qinling Shan (**Fig. 10**; Feng et al., 2021; 2022). A similar change in provenance may explain the appearance of magnetite in the Xining Basin. However, the single to pseudo-single domain magnetic properties that we observe indicate that the magnetite in the Xining Basin is very fine grained and unlikely to withstand long-term sedimentary transport.

Alternatively, increased precipitation could have resulted in the formation and preservation of pedogenic magnetite as widely observed in the paleosols of the Chinese Loess Plateau (e.g. Ahmed and Maher, 2018; Deng et al., 2004; Maher and Taylor, 1988). This could also explain the higher organic content corresponding with the higher magnetic susceptibilities in the middle and upper Qijiachuan Formation and gradual decrease in susceptibility in the overlying Honggou Formation which has been previously linked to drying (Fang et al., 2015). A pedogenic origin for some of the particles in this interval is supported by frequency-dependent susceptibility data indicating the occurrence of ultrafine magnetic particles at the superparamagnetic to single domain transition (Fang et al., 2015). However, we note that the shift to higher magnetic susceptibility also corresponds to higher NRM (**Fig. S1**), which

indicates a significant contribution of single domain grains as well. The higher accumulation rates observed in this interval (**Fig. 9**) may have played a role in reducing the time of subaerial exposure for the sediments. This could have improved the preservation of magnetite by both reducing the dissolution and oxidation of the magnetite minerals (e.g. Fang et al., 2015). The fine-grained hematite may have been formed by the oxidation of magnetite or the transformation of iron hydroxides. Scanning Electron Microscope (SEM) imaging indicates the presence of numerous small iron oxides (<2 to 5 µm) but our observations are not sufficient to confirm a detrital or authigenic origin of these iron oxides.

Yet regardless of the exact magnetite origin, we suggest that its abrupt appearance following the underlying inconsistent magnetostratigraphy might indicate the presence of an unconformity at the base of the middle Qijiachuan Formation. A more distinct angular unconformity is observed further below between the Minhe and Qijiachuan Formations (**Fig. 3 E**). This unconformity can be recognized throughout the basin (He et al., 2021; QBGMR; 1985), although in some places less obvious as a disconformity with parallel bedding such as in the Sanhe, Dazhai and Ledu sections (**Fig. 2**). Age constraints on the lower Qijiachuan Formation occurring between these unconformities are limited, but ostracods and palynomorphs suggest a Cretaceous to Paleocene age (Horton et al., 2004). We also note that the accumulation rates in the early Honggou Formation are extremely low (~0.5 cm/ka in C23n and C22r; **Fig. 9**), which may indicate additional minor unconformities, even though we do not observe any lithological evidence for this.

In conclusion, the early Paleogene strata of the Xining Basin are marked by at least one, but possibly several unconformities and variable sedimentation rates, both in time and laterally between sections. This infill pattern is in stark contrast to the stable accumulation rates of 2-3 cm/ka observed in the overlying Paleogene and Neogene strata (Dai et al., 2006; Meijer et al., 2019; Xiao et al., 2012; Yang F et al., 2019; Zhang et al., 2017). In the following we will discuss this infill pattern in view of the regional tectonic setting.

Accepted Article

Accepted Article

5.2 Tectonic implications

The northeastern Tibetan Plateau is located between two tectonic regimes that dominate the region (e.g. Ratschbacher et al., 2003; Zhuang et al., 2018; Zhang et al., 2019). On the one hand is the subduction of the Pacific Plate resulting in NW-SE extension and forming multiple extensional basins in eastern China (e.g. Gilder et al., 1991; Ren et al., 2002). This extensional domain may have extended further inland resulting in the formation of grabens around the Ordos block and in northeastern Tibet (**Fig. 10**; Fan et al., 2019; Mercier et al., 2013; Ratschbacher et al., 2003; Wang et al., 2013; Zhang et al., 2003). On the other hand is the India-Asia collision resulting in SW to NE shortening and, mostly left-lateral, strike slip faulting (**Fig. 10**; e.g. Ratschbacher et al., 2003; Taponnier et al., 2001; Yuan et al., 2013; Zuza et al., 2016). The far-field effects of the collision may have propagated quickly to the northeastern margin of the Tibetan Plateau (e.g. Clark et al., 2010; Jolivet et al., 2001; Liu et al., 2013; Yin et al., 2008; Yuan et al., 2013), soon after the collision starting at ~60 Ma (e.g. Hu et al., 2016; Kapp and DeCelles, 2019). This has been supported by numerous thermochronological studies indicating early Eocene exhumation in various mountain ranges including the Altyn Tagh, Qilian Shan, East Kunlun Shan and Western Qinling Shan (**Fig. 10**; Clark et al., 2010; He et al., 2017; 2018; 2020; Jolivet et al., 2001; Li et al., 2020; Staisch et al., 2020). The formation of several flexural basins has been linked to this tectonic loading such as the Chaka Basin at 11 Ma (Zhang et al., 2012), the Gonghe Basin at 20 Ma (Craddock et al., 2011) and the Qaidam Basin (**Fig. 10**; Wang et al., 2021) starting either at 51 Ma ("old ages" model; e.g. Ji et al., 2017; Yin et al., 2008) or at 25.5 Ma ("young ages" model; Nie et al., 2020; Wang et al., 2017).

It remains debated whether the Paleogene Xining Basin formed due to flexure like the Qaidam Basin located in the west or in an extensional setting similar to the grabens in the east. Other sub-basins of the Longzhong Basin such as the neighboring Xunhua-Guide and Linxia Basins

Accepted Article

show a thickening of the Neogene strata towards the Western Qinling Shan in the south which supports a developing foredeep due to tectonic loading (**Fig. 10**; **11 A**; Fang et al., 2003; 2016; Liu et al., 2013). Increased exhumation of the Western Qinling Shan started already at ~50-45 Ma (Clark et al., 2010; Duvall et al., 2011), which closely corresponds with the onset of deposition in the Linxia Basin at ~54-53 Ma (C24n; Feng et al., 2022) and possibly the Xining Basin at >53 Ma. However, we note that the infill pattern of the Xining Basin is not characteristic of a typical foreland basin. Accumulation rates are relatively low throughout the Paleogene (~3 cm /kyr, except for the early Eocene), and no coarsening upward trend typical for foredeep propagation (e.g. DeCelles and Giles, 1996) is observed. Increasing accumulation rates and coarsening lithologies only occur ~40 million years later during the Neogene uplift of various mountain ranges segmenting the Longzhong Basin (Fang et al., 2016; He et al., 2021; Hough et al., 2014; Lease et al., 2011; 2012; Xiao et al., 2012; Yang et al., 2017).

In contrast, extensional basins are characterised by numerous smaller depocenters during the initiation phase, before coalescing into a larger and more stable basin during the later stages (Gawthorpe and Leeder, 2000). This model better explains the local and variable accumulation rates observed in the Xining Basin between 52.9 and 49.7 Ma, followed by low but stable accumulation of the overlying strata. Our study therefore supports an extensional origin for the Paleogene Xining Basin, which could be linked to the development of nearby Eocene grabens such as the Weihe Basin and other half-grabens in the eastern part of the Qinling Shan (**Fig. 10;** Chen et al., 2021; Liu J. et al., 2013; Ratschbacher et al., 2003). However, the exact dynamics driving this extension remain unclear. Fan et al. (2019) report various normal faults in the Xining strata indicating a NW-SE extensional regime (**Fig. 11 B**; Fan et al., 2019). Key features are the east and west Shenjiaxia faults and normal faults in the overlying mudrocks, both located ~2 km south of the Ledu section (Fan et al., 2019). However, here we note that these faults and mudrocks are not part of the Paleogene Xining Group as suggested by Fan et al. (2019), but likely of Cretaceous age because they occur only in the strata below the

sandstones of the Minhe Formation. These observations are consistent with an older Cretaceous phase of extension in the Xining Basin (Horton et al., 2004), which is well-documented throughout the region and linked to back-arc spreading and/or intracontinental rifting (e.g. Gilder et al., 1991; Ren et al., 2002).

Wang et al. (2013; 2016) have proposed a renewed phase of SW to NE extension during the Eocene. This would have resulted in right-lateral movement of the basin-bounding faults thereby forming the Longzhong Basin (**Fig. 11 C**), before the faults were inverted to the left-lateral sense of movement observed today (**Fig. 10**). This is based on structural and stratigraphic observations from the northeastern margin of the Longzhong Basin and supported by the clockwise rotation observed in the paleomagnetic data of the Xining Basin between 40 and 29 Ma (Dupont-Nivet et al., 2004; 2008b). Both Fan et al. (2019) and Wang et al. (2013) suggest that this Eocene extension is driven by the slowdown of convergence and possibly slab rollback of the Pacific Plate (Northrup et al., 1995; Zhuang et al., 2018). Alternatively, the far-field effects of the India-Asia collision could have driven the differential rotation of crustal blocks thereby forming the Xining Basin through transtension (**Fig. 11 D**; Zhang et al., 2016). The continued growth of the northern Tibetan Plateau would have played an increasingly important role throughout the late Paleogene and Neogene and may have driven additional flexural or transtensional subsidence thereby enlargening the Longzhong Basin (Fang et al., 2003; 2016; Lease et al., 2012; Liu et al., 2013; Wang et al., 2016).

Accepted Article

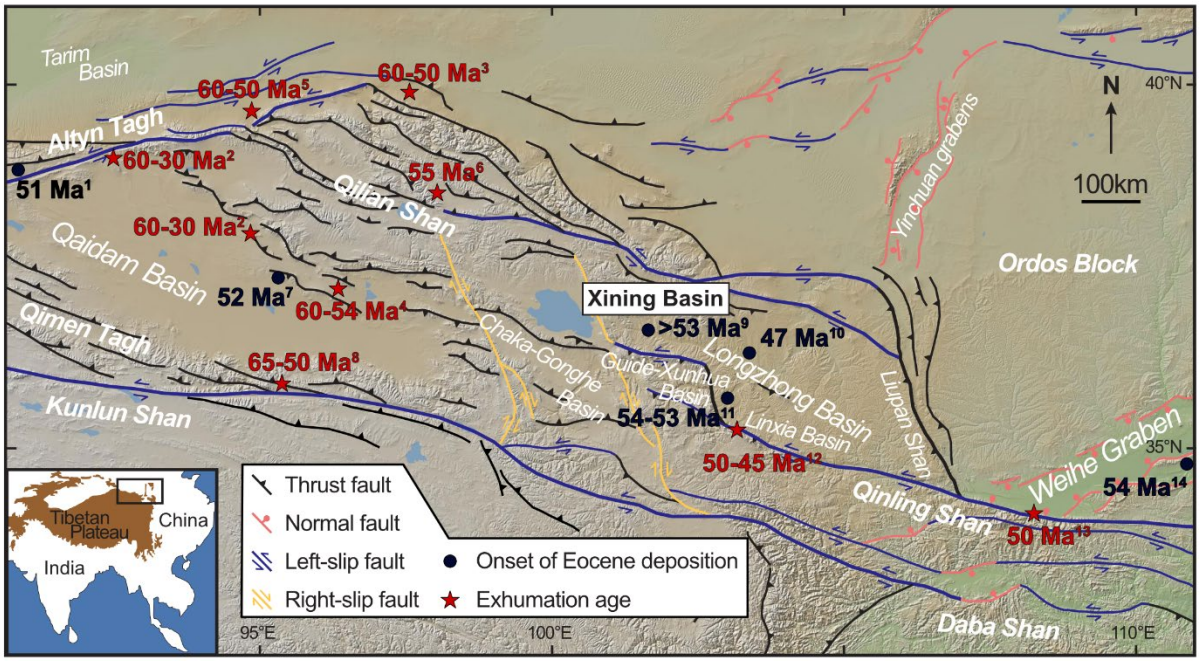


Fig. 10. Map of the northeastern Tibetan Plateau showing tectonic events during the early Eocene: 1) Li et al. (2018); 2) Jolivet et al. (2001); 3) He et al. (2017); 4) He et al. (2018); 5) He et al. (2020); 6) Li et al. (2020); 7) Ji et al. (2017); 8) Staisch et al. (2020); 9) He et al. (2021) and this study; 10) Wang et al. (2016); 11) Feng et al. (2021); 12) Clark et al. (2010); 13) Liu et al. (2013); 14) Chen et al. (2021). Modern-day topographic base map is from the GeoMapApp software (Ryan et al., 2009) available at http://www.geomapapp.org/. The faults are redrawn from Zuza et al. (2016) and references therein.

Accepted Article

Accepted Article

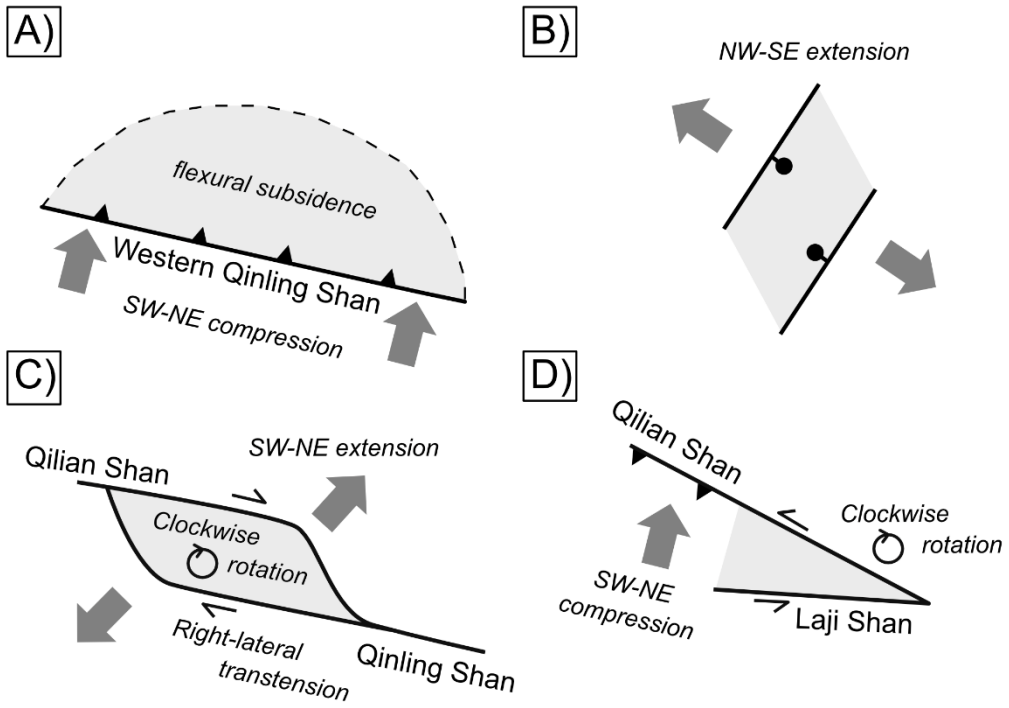


Fig. 11. Tectonic models for the origin of the Xining Basin: A) Foreland basin of the Western Qinling Shan (Fang et al., 2003; 2016; He et al., 2021; Liu et al., 2013). B) Extensional basin due to normal faulting (Fan et al., 2019). C) Right-lateral transtensional basin due to SW-NE extension (Wang et al., 2013; 2016). D) Left-lateral transtensional basin due to differential rotation of crustal blocks (Zhang et al., 2016).

6. Conclusion

The early Eocene sections of the Xining Basin reveal a complex stratigraphy with lateral variability and unconformities. However, by using litho- and magnetostratigraphic correlations throughout the basin, we were able to extend the age model down to the early Eocene at 53.0 Ma (C24n.1r). The stratigraphy reveals an unstable pattern of basin infill between 52.9 and 49.7 Ma (C23n to C22r) with variable accumulation rates ranging from 0.5 to 8 cm/ka. This is in stark contrast to the stable accumulation rates of 2 to 3 cm/ka observed in the overlying strata.

Accepted Article

This pattern of slow basin infill is not characteristic of a foreland basin as previously suggested (e.g. Liu et al., 2013; He et al., 2021) but supports an extensional origin of the Xining Basin. Currently, multiple extensional models exist including NW-SE normal faulting (Fan et al., 2019) and right-lateral transtension (Wang et al., 2013; 2016) both related to the subduction of the Pacific Plate, as well as transtension due to far-field effects of the India-Asia collision and the differential rotation of crustal blocks (Zhang et al., 2016). The Xining Basin is located between these tectonic domains and more detailed structural analyses are required to identify the associated faults, date their motion and test the driving mechanisms for extension. Nevertheless, our results elucidate the early tectonic evolution of the Cenozoic Xining Basin and highlight the need for basin-scale analyses to deal with the complex stratigraphy of intracontinental basins (e.g. Fang et al., 2016). Furthermore, we provide a detailed lithostratigraphy and age model for future tectonic, sedimentological, palynological and paleo-environmental studies in the basin.

Data Availability Statement

Raw paleomagnetic data is available at earthref.org/MagIC/19501. ChRM directions, VGP's and U-Pb data are available in the Supporting Information.

Acknowledgements

This study was funded by the ERC consolidator grant MAGIC 649081 to GDN and through the VeWA consortium by the LOEWE programme of the Hessen Ministry of Higher Education, Research and the Arts, Germany. We thank Meimei Xiao, Yang Zhang and Femke Saulus for their support in the field and in the lab. We also thank Richard Heermance and two anonymous reviewers for their helpful comments.

Accepted Article

References

Abels, H. A., Dupont-Nivet, G., Xiao, G., Bosboom, R., & Krijgsman, W. (2011). Step-wise change of Asian interior climate preceding the Eocene–Oligocene Transition (EOT). *Palaeogeography, Palaeoclimatology, Palaeoecology*, *299*(3), 399-412. https://doi.org/10.1016/j.palaeo.2010.11.028

Ahmed, I. A., & Maher, B. A. (2018). Identification and paleoclimatic significance of magnetite nanoparticles in soils. *Proceedings of the National Academy of Sciences, 115*(8), 1736-1741. https://doi.org/10.1073/pnas.1719186115

Bosboom, R. E., Abels, H. A., Hoorn, C., van den Berg, B. C., Guo, Z., & Dupont-Nivet, G. (2014). Aridification in continental Asia after the Middle Eocene Climatic Optimum (MECO). *Earth and Planetary Science Letters*, *389*, 34-42. https://doi.org/10.1016/j.epsl.2013.12.014

Bureau of Geological and Mineral Resources of Qinghai Province (BGMRQP), 1965. Regional geological survey reports of Ledu sheet (1:200000), Qinghai Province, P.R. China (in Chinese).

Chen, X., Dong, S., Shi, W., Zuza, A. V., Li, Z., Chen, P., Liu, J., Hu, J.& Han, B. (2021). Magnetostratigraphic ages of the Cenozoic Weihe and Shanxi Grabens in North China and their tectonic implications. Tectonophysics, 813, 228914. https://doi.org/10.1016/j.tecto.2021.228914

Cheng, F., Jolivet, M., Guo, Z., Wang, L., Zhang, C., & Li, X. (2021). Cenozoic evolution of the Qaidam basin and implications for the growth of the northern Tibetan plateau: A review. *Earth-Science Reviews*, 103730. https://doi.org/10.1016/j.earscirev.2021.103730

Clark, M. K., Farley, K. A., Zheng, D., Wang, Z., & Duvall, A. R. (2010). Early Cenozoic faulting of the northern Tibetan Plateau margin from apatite (U–Th)/He ages. *Earth and Planetary Science Letters*, *296*(1), 78-88. https://doi.org/10.1016/j.epsl.2010.04.051

Cong, F., Tian, J., Hao, F., Licht, A., Liu, Y., Cao, Z., & Eiler, J. M. (2021). A Thermal Pulse Induced by a Permian Mantle Plume in the Tarim Basin, Northwest China: Constraints

Accepted Article

From Clumped Isotope Thermometry and In Situ Calcite U-Pb Dating. *Journal of Geophysical Research: Solid Earth, 126*(4), e2020JB020636. https://doi.org/10.1029/2020JB020636

Craddock, W., Kirby, E., & Zhang, H. (2011). Late Miocene–Pliocene range growth in the interior of the northeastern Tibetan Plateau. *Lithosphere, 3*(6), 420-438. https://doi.org/10.1130/L159.1

Dai, S., Fang, X., Dupont-Nivet, G., Song, C., Gao, J., Krijgsman, W., Langereis, C. & Zhang, W. (2006). Magnetostratigraphy of Cenozoic sediments from the Xining Basin: Tectonic implications for the northeastern Tibetan Plateau. *Journal of Geophysical Research: Solid Earth*, *111*(B11). https://doi.org/10.1029/2005JB004187

DeCelles, P. G., & Giles, K. A. (1996). Foreland basin systems. *Basin research, 8*(2), 105-123. https://doi.org/10.1046/j.1365-2117.1996.01491.x

Deng, C., Zhu, R., Verosub, K. L., Singer, M. J., & Vidic, N. J. (2004). Mineral magnetic properties of loess/paleosol couplets of the central loess plateau of China over the last 1.2 Myr. Journal of Geophysical Research: Solid Earth, 109(B1). https://doi.org/10.1029/2003JB002532

Dupont-Nivet, G., Horton, B. K., Butler, R. F., Wang, J., Zhou, J., & Waanders, G. L. (2004). Paleogene clockwise tectonic rotation of the Xining-Lanzhou region, northeastern Tibetan Plateau. Journal of Geophysical Research: *Solid Earth, 109*(B4). https://doi.org/10.1029/2003JB002620

Dupont-Nivet, G., Krijgsman, W., Langereis, C. G., Abels, H. A., Dai, S., & Fang, X. (2007). Tibetan plateau aridification linked to global cooling at the Eocene–Oligocene transition. *Nature*, *445*(7128), 635-638.

Dupont-Nivet, G., Hoorn, C., & Konert, M. (2008a). Tibetan uplift prior to the Eocene-Oligocene climate transition: Evidence from pollen analysis of the Xining Basin. *Geology, 36*(12), 987-990. https://doi.org/10.1130/G25063A.1

Accepted Article

Dupont-Nivet, G., Dai, S., Fang, X., Krijgsman, W., Erens, V., Reitsma, M. & Langereis, C. (2008b). Timing and distribution of tectonic rotations in the northeastern Tibetan Plateau. *Investigations into the Tectonics of the Tibetan Plateau, 444*, 73-87.

Duvall, A. R., Clark, M. K., van der Pluijm, B. A., & Li, C. (2011). Direct dating of Eocene reverse faulting in northeastern Tibet using Ar-dating of fault clays and low-temperature thermochronometry. *Earth and Planetary Science Letters, 304*(3-4), 520-526. https://doi.org/10.1016/j.epsl.2011.02.028

Fan, L. G., Meng, Q. R., Wu, G. L., Wei, H. H., Du, Z. M., & Wang, E. (2019). Paleogene crustal extension in the eastern segment of the NE Tibetan plateau. Earth and Planetary Science Letters, 514, 62-74. https://doi.org/10.1016/j.epsl.2019.02.036

Fang, X., Garzione, C., Van der Voo, R., Li, J., & Fan, M. (2003). Flexural subsidence by 29 Ma on the NE edge of Tibet from the magnetostratigraphy of Linxia Basin, China. *Earth and Planetary Science Letters, 210*(3-4), 545-560. https://doi.org/10.1016/S0012-821X(03)00142-0

Fang, X., Zan, J., Appel, E., Lu, Y., Song, C., Dai, S., & Tuo, S. (2015). An Eocene–Miocene continuous rock magnetic record from the sediments in the Xining Basin, NW China: indication for Cenozoic persistent drying driven by global cooling and Tibetan Plateau uplift. Geophysical Journal International, 201(1), 78-89. https://doi.org/10.1093/gji/ggv002

Fang, X., Wang, J., Zhang, W., Zan, J., Song, C., Yan, M., Appel, E., Zhang, T., Wu, Fuli, Yang, Y. & Lu, Y. (2016). Tectonosedimentary evolution model of an intracontinental flexural (foreland) basin for paleoclimatic research. *Global and Planetary Change, 145*, 78-97. https://doi.org/10.1016/j.gloplacha.2016.08.015

Fang, X., Fang, Y., Zan, J., Zhang, W., Song, C., Appel, E., Meng, Q., Miao, Y., Dai, .S, Lu, Y. & Zhang, T. (2019). Cenozoic magnetostratigraphy of the Xining Basin, NE Tibetan Plateau, and its constraints on paleontological, sedimentological and tectonomorphological evolution. *Earth-science Reviews, 190,* 460-485. https://doi.org/10.1016/j.earscirev.2019.01.021

Accepted Article

Fang, X., Galy, A., Yang, Y., Zhang, W., Ye, C., & Song, C. (2019). Paleogene global cooling–induced temperature feedback on chemical weathering, as recorded in the northern Tibetan Plateau. Geology, 47(10), 992-996.

Feng, Z., Zhang, W., Zhang, T., Fang, X., Zan, J., Yan, M., Song, C., Li, T., Ning, W. & Wang, H. (2021). Early-Middle Eocene Hydroclimate Variations Recorded by Environmental Magnetism in the Linxia Basin, NE Tibetan Plateau. Paleoceanography and Paleoclimatology, 36(11), e2021PA004338. https://doi.org/10.1029/2021PA004338

Feng, Z., Zhang, W., Fang, X., Zan, J., Zhang, T., Song, C., & Yan, M. (2022). Eocene deformation of the NE Tibetan Plateau: Indications from magnetostratigraphic constraints on the oldest sedimentary sequence in the Linxia Basin. *Gondwana Research, 101*, 77-93. https://doi.org/10.1016/j.gr.2021.07.027

Fisher, R. (1953). Dispersion on a sphere. In Proceedings of the Royal Society of London A: Mathematical, Physical and Engineering Sciences (Vol. 217, No. 1130, pp. 295-305). The Royal Society. DOI: 10.1098/rspa.1953.0064

Gawthorpe, R. L., & Leeder, M. R. (2000). Tectono-sedimentary evolution of active extensional basins. Basin Research, 12(3-4), 195-218. https://doi.org/10.1111/j.1365-2117.2000.00121.x

Gilder, S. A., Keller, G. R., Luo, M., & Goodell, P. C. (1991). Eastern Asia and the western Pacific timing and spatial distribution of rifting in China. *Tectonophysics, 197*(2-4), 225-243. https://doi.org/10.1016/0040-1951(91)90043-RGet

He, C. C., Zhang, Y. Q., Li, S. K., Wang, K., & Ji, J. Q. (2021). Magnetostratigraphic study of a Late Cretaceous− Paleogene succession in the eastern Xining basin, NE Tibet: Constraint on the timing of major tectonic events in response to the India-Eurasia collision. *GSA Bulletin*. https://doi.org/10.1130/B35874.1

He, P., C. Song, Y. Wang, L. Chen, P. Chang, Q. Wang, and B. Ren (2017), Cenozoic exhumation in the Qilian Shan, northeastern Tibetan Plateau: Evidence from detrital fission track thermochronology in the Jiuquan Basin, *J. Geophys. Res. Solid Earth, 122*, 6910–6927, doi:10.1002/2017JB014216

Accepted Article

He, P., Song, C., Wang, Y., Meng, Q., Chen, L., Yao, L., HUang, R., Feng, W. & Chen, S. (2018). Cenozoic deformation history of the Qilian Shan (northeastern Tibetan Plateau) constrained by detrital apatite fission-track thermochronology in the northeastern Qaidam Basin. *Tectonophysics, 749*, 1-11. https://doi.org/10.1016/j.tecto.2018.10.017

He, P., Song, C., Wang, Y., Meng, Q., Wang, D., Feng, Y., Chen, L. & Feng, W. (2020). Early Cenozoic exhumation in the Qilian Shan, northeastern margin of the Tibetan Plateau: Insights from detrital apatite fission track thermochronology. *Terra Nova, 32*(6), 415-424. https://doi.org/10.1111/ter.12478

Hoorn, C., Straathof, J., Abels, H. A., Xu, Y., Utescher, T., & Dupont-Nivet, G. (2012). A late Eocene palynological record of climate change and Tibetan Plateau uplift (Xining Basin, China). *Palaeogeography, Palaeoclimatology, Palaeoecology, 344*, 16-38. https://doi.org/10.1016/j.palaeo.2012.05.011

Horton, B. K., Dupont-Nivet, G., Zhou, J., Waanders, G. L., Butler, R. F., & Wang, J. (2004). Mesozoic-Cenozoic evolution of the Xining-Minhe and Dangchang basins, northeastern Tibetan Plateau: Magnetostratigraphic and biostratigraphic results. *Journal of Geophysical Research: Solid Earth*, *109*(B4). https://doi.org/10.1029/2003JB002913

Hough, B. G., Garzione, C. N., Wang, Z., Lease, R. O., Nie, J., Horton, B. K., & Hoke, G. D. (2014). Timing and spatial patterns of basin segmentation and climate change in northeastern Tibet. Toward an Improved Understanding of Uplift Mechanisms and the Elevation History of the Tibetan Plateau: *Geological Society of America Special Paper, 507*, 129-153.

Hu, X., Garzanti, E., Wang, J., Huang, W., An, W., & Webb, A. (2016). The timing of India-Asia collision onset–Facts, theories, controversies. *Earth-Science Reviews, 160*, 264-299. https://doi.org/10.1016/j.earscirev.2016.07.014

Ji, J., Zhang, K., Clift, P. D., Zhuang, G., Song, B., Ke, X., & Xu, Y. (2017). High-resolution magnetostratigraphic study of the Paleogene-Neogene strata in the Northern Qaidam Basin: Implications for the growth of the Northeastern Tibetan Plateau. *Gondwana Research, 46*, 141-155. https://doi.org/10.1016/j.gr.2017.02.015

Accepted Article

Jolivet, M., Brunel, M., Seward, D., Xu, Z., Yang, J., Roger, F., Tapponnier, P., Malavieille, J., Arnaud, N. & Wu, C. (2001). Mesozoic and Cenozoic tectonics of the northern edge of the Tibetan plateau: fission-track constraints. *Tectonophysics, 343*(1-2), 111-134. https://doi.org/10.1016/S0040-1951(01)00196-2

Kapp, P., & DeCelles, P. G. (2019). Mesozoic–Cenozoic geological evolution of the Himalayan-Tibetan orogen and working tectonic hypotheses. *American Journal of Science, 319*(3), 159-254. https://doi.org/10.2475/03.2019.01

Kirschvink, J. L. (1980). The least-squares line and plane and the analysis of palaeomagnetic data. *Geophysical Journal International*, *62*(3), 699-718. https://doi.org/10.1111/j.1365-246X.1980.tb02601.x

Lease, R. O., Burbank, D. W., Clark, M. K., Farley, K. A., Zheng, D., & Zhang, H. (2011). Middle Miocene reorganization of deformation along the northeastern Tibetan Plateau. *Geology, 39*(4), 359-362. https://doi.org/10.1130/G31356.1

Lease, R. O., Burbank, D. W., Hough, B., Wang, Z., & Yuan, D. (2012). Pulsed Miocene range growth in northeastern Tibet: Insights from Xunhua Basin magnetostratigraphy and provenance. *Bulletin, 124*(5-6), 657-677. https://doi.org/10.1130/B30524.1

Li, J. X., Yue, L. P., Roberts, A. P., Hirt, A. M., Pan, F., Guo, L., Xu., Y., Xi, R. G., Guo, L., Qiang, X. K., Gai, C. C., Jiang, Z. X., Sun, Z. M., & Liu, Q. S. (2018). Global cooling and enhanced Eocene Asian mid-latitude interior aridity. *Nature communications, 9*(1), 3026. https://doi.org/10.1038/s41467-018-05415-x

Li, B., Zuza, A. V., Chen, X., Hu, D., Shao, Z., Qi, B., Wang, Z., Levy, D. A. & Xiong, X. (2020). Cenozoic multi-phase deformation in the Qilian Shan and out-of-sequence development of the northern Tibetan Plateau. *Tectonophysics, 782*, 228423. https://doi.org/10.1016/j.tecto.2020.228423

Licht, A., Van Cappelle, M., Abels, H. A., Ladant, J. B., Trabucho-Alexandre, J., France-Lanord, C., Donnadieu, Y., Vandenberghe, J., Rigaudier, T., Lécuyer, C., Terry Jr, D., Adriaens, R., Boura, A., Guo, Z., Aung Naing Soe, Quade, J., Dupont-Nivet, G. & Jaeger,

Accepted Article

J.-J. (2014). Asian monsoons in a late Eocene greenhouse world. *Nature, 513*(7519), 501-506. https://doi.org/10.1038/nature13704

Licht, A., Dupont-Nivet, G., Pullen, A., Kapp, P., Abels, H. A., Lai, Z., Guo, Z., Abell, J. & Giesler, D. (2016). Resilience of the Asian atmospheric circulation shown by Paleogene dust provenance. *Nature communications, 7*, 12390. https://doi.org/10.1038/ncomms12390

Licht, A., Dupont-Nivet, G., Meijer, N., Rugenstein, J. C., Schauer, A., Fiebig, J., Mulch, A., Hoorn, C. & Guo, Z. (2020). Decline of soil respiration in northeastern Tibet through the transition into the Oligocene icehouse. *Palaeogeography, Palaeoclimatology, Palaeoecology, 560*, 110016. https://doi.org/10.1016/j.palaeo.2020.110016

Licht, A., Win, Z., Westerweel, J., Cogné, N., Morley, C. K., Chantraprasert, S., Poblete F., Ugrai, T., Nelson, B., Aung, D. W. & Dupont-Nivet, G. (2020). Magmatic history of central Myanmar and implications for the evolution of the Burma Terrane. *Gondwana Research, 87*, 303-319. https://doi.org/10.1016/j.gr.2020.06.016

Liu, J., Zhang, P., Lease, R. O., Zheng, D., Wan, J., Wang, W., & Zhang, H. (2013). Eocene onset and late Miocene acceleration of Cenozoic intracontinental extension in the North Qinling range–Weihe graben: Insights from apatite fission track thermochronology. *Tectonophysics, 584*, 281-296. https://doi.org/10.1016/j.tecto.2012.01.025

Liu, S., Zhang, G., Pan, F., Zhang, H., Wang, P., Wang, K., & Wang, Y. (2013). Timing of Xunhua and Guide basin development and growth of the northeastern Tibetan Plateau, China. *Basin Research, 25*(1), 74-96. https://doi.org/10.1111/j.1365-2117.2012.00548.x

Maher, B. A., & Taylor, R. M. (1988). Formation of ultrafine-grained magnetite in soils. *Nature, 336*(6197), 368-370. https://doi.org/10.1038/336368a0

McFadden, P. L., & McElhinny, M. W. (1990). Classification of the reversal test in palaeomagnetism. *Geophysical Journal International*, *103*(3), 725-729. https://doi.org/10.1111/j.1365-246X.1990.tb05683.x

Meijer, N., Dupont-Nivet, G., Abels, H. A., Kaya, M. Y., Licht, A., Xiao, M., Zhang, Y., Roperch, P., Poujol, M., Lai, Z. & Guo, Z. (2019). Central Asian moisture modulated by

Accepted Article

proto-Paratethys Sea incursions since the early Eocene. *Earth and Planetary Science Letters, 510*, 73-84. https://doi.org/10.1016/j.epsl.2018.12.031

Meijer, N., Dupont-Nivet, G., Barbolini, N., Woutersen, A., Rohrmann, A., Zhang, Y., Liu X. J., Licht, A., Abels, H. A., Hoorn, C., Tjallingii, R., Andermann, C., Dietze, M. & Nowaczyk, N. (2021). Loess-Like Dust Appearance at 40 Ma in Central China. *Paleoceanography and paleoclimatology, 36*(3), e2020PA003993. https://doi.org/10.1029/2020PA003993

Mercier, J. L., Vergely, P., Zhang, Y. Q., Hou, M. J., Bellier, O., & Wang, Y. M. (2013). Structural records of the late Cretaceous–Cenozoic extension in Eastern China and the kinematics of the Southern Tan-Lu and Qinling fault zone (Anhui and Shaanxi provinces, PR China). *Tectonophysics, 582*, 50-75. https://doi.org/10.1016/j.tecto.2012.09.015

Nie, J., Ren, X., Saylor, J. E., Su, Q., Horton, B. K., Bush, M. A., Chen, W. & Pfaff, K. (2020). Magnetic polarity stratigraphy, provenance, and paleoclimate analysis of Cenozoic strata in the Qaidam Basin, NE Tibetan Plateau. GSA Bulletin, 132(1-2), 310-320. https://doi.org/10.1130/B35175.1

North, C. P., & Davidson, S. K. (2012). Unconfined alluvial flow processes: recognition and interpretation of their deposits, and the significance for palaeogeographic reconstruction. *Earth-Science Reviews, 111*(1), 199-223. https://doi.org/10.1016/j.earscirev.2011.11.008

Northrup, C. J., Royden, L. H., & Burchfiel, B. C. (1995). Motion of the Pacific plate relative to Eurasia and its potential relation to Cenozoic extension along the eastern margin of Eurasia. *Geology, 23*(8), 719-722. https://doi.org/10.1130/0091-7613(1995)023<0719:MOTPPR>2.3.CO;2

Ogg, J. G. (2020). Geomagnetic polarity time scale. In *Geologic Time Scale 2020* (pp. 159-192). Elsevier. https://doi.org/10.1016/B978-0-12-824360-2.00005-X

Page, M., Licht, A., Dupont-Nivet, G., Meijer, N., Barbolini, N., Hoorn, C., Schauer, A., Huntington, K., Bajnai, D., Fiebig, J. & Mulch, A. (2019). Synchronous cooling and

Accepted Article

decline in monsoonal rainfall in northeastern Tibet during the fall into the Oligocene icehouse. *Geology, 47*(3), 203-206. https://doi.org/10.1130/G45480.1

Qinghai Bureau of Geology and Mineral Resources (QBGMR) (1985), Geologic maps of the Duoba, Gaodian, Tianjiazai, and Xining regions (4 sheets), with regional geologic report (1:50,000 scale), 199 pp., Xining, China.

Ratschbacher, L., Hacker, B. R., Calvert, A., Webb, L. E., Grimmer, J. C., McWilliams, M. O., Ireland, T., Dong, S. & Hu, J. (2003). Tectonics of the Qinling (Central China): tectonostratigraphy, geochronology, and deformation history. Tectonophysics, 366(1-2), 1-53. https://doi.org/10.1016/S0040-1951(03)00053-2

Ren, J., Tamaki, K., Li, S., & Junxia, Z. (2002). Late Mesozoic and Cenozoic rifting and its dynamic setting in Eastern China and adjacent areas. *Tectonophysics*, 344(3-4), 175-205. https://doi.org/10.1016/S0040-1951(01)00271-2

Roberts, A. P., Cui, Y., & Verosub, K. L. (1995). Wasp-waisted hysteresis loops: Mineral magnetic characteristics and discrimination of components in mixed magnetic systems. Journal of Geophysical Research: Solid Earth, 100(B9), 17909-17924. https://doi.org/10.1029/95JB00672

Ruan, X., Yang, Y., Galy, A., Fang, X., Jin, Z., Zhang, F., Yang, R., Deng, L., Meng, Q., Ye, C., & Zhang, W. (2019). Evidence for early (≥ 12.7 Ma) eolian dust impact on river chemistry in the northeastern Tibetan Plateau. *Earth and Planetary Science Letters, 515*, 79-89. https://doi.org/10.1016/j.epsl.2019.03.022

Ryan, W. B. F., S.M. Carbotte, J. Coplan, S. O'Hara, A. Melkonian, R. Arko, R.A. Weissel, V. Ferrini, A. Goodwillie, F. Nitsche, J. Bonczkowski, and R. Zemsky (2009), Global Multi-Resolution Topography (GMRT) synthesis data set, *Geochem. Geophys. Geosyst., 10*, Q03014, https://doi.org/10.1029/2008GC002332.

Smoot, J. P., & Lowenstein, T. K. (1991). Depositional environments of non-marine evaporites. In *Developments in sedimentology* (Vol. 50, pp. 189-347). Elsevier. https://doi.org/10.1016/S0070-4571(08)70261-9

Accepted Article

Staisch, L. M., Niemi, N. A., Clark, M. K., & Chang, H. (2020). The Cenozoic evolution of crustal shortening and left-lateral shear in the central East Kunlun Shan: Implications for the uplift history of the Tibetan Plateau. *Tectonics, 39*, e2020TC006065. https://doi.org/10.1029/2020TC006065

Talbot, M. R., Holm, K., & Williams, M. A. J. (1994). Sedimentation in low-gradient desert margin systems: A comparison of the Late Triassic of northwest Somerset (England) and the late Quaternary of east-central Australia. *Geological Society of America Special Papers, 289*, 97-117.

Tapponnier, P., Zhiqin, X., Roger, F., Meyer, B., Arnaud, N., Wittlinger, G., & Jingsui, Y. (2001). Oblique stepwise rise and growth of the Tibet Plateau. *Science, 294*(5547), 1671-1677. https://doi.org/10.1126/science.105978

Wang, W., Kirby, E., Peizhen, Z., Dewen, Z., Guangliang, Z., Huiping, Z., Wenjun, Z. & Chizhang, C. (2013). Tertiary basin evolution along the northeastern margin of the Tibetan Plateau: Evidence for basin formation during Oligocene transtension. *Bulletin, 125*(3-4), 377-400. https://doi.org/10.1130/B30611.1

Wang, W., Zhang, P., Liu, C., Zheng, D., Yu, J., Zheng, W., Wang, Y., Zhang, H. & Chen, X. (2016). Pulsed growth of the West Qinling at~ 30 Ma in northeastern Tibet: Evidence from Lanzhou Basin magnetostratigraphy and provenance. *Journal of Geophysical Research: Solid Earth, 121*(11), 7754-7774. https://doi.org/10.1002/2016JB013279

Wang, L., Cheng, F., Zuza, A. V., Jolivet, M., Liu, Y., Guo, Z., Li, X. & Zhang, C. (2021). Diachronous growth of the northern Tibetan plateau derived from flexural modeling. Geophysical Research Letters, 48(8), e2020GL092346. https://doi.org/10.1029/2020GL092346

Westerhold, T., Marwan, N., Drury, A. J., Liebrand, D., Agnini, C., Anagnostou, E., Barnet, J. S. K., Bohaty, S. M., De Vleeschouwer, D., Florindo, F., Frederichs, T., Hodell, D. A., Holbourn, A. E., Kroon, D., Lauretano, V., Littler, K., Lourens, L. J., Lyle, M., Pälike, H., Röhl, U., Tian, J., Wilkens, R. H., Wilson, P. A. & Zachos, J. C. (2020). An astronomically

Accepted Article

dated record of Earth's climate and its predictability over the last 66 million years. Science, 369(6509), 1383-1387. https://doi.org/10.1126/science.aba6853

Xiao, G., Guo, Z., Dupont-Nivet, G., Lu, H., Wu, N., Ge, J., Hao, Q., Peng, S., Li, F., Abels, H. A. & Zhang, K. (2012). Evidence for northeastern Tibetan Plateau uplift between 25 and 20Ma in the sedimentary archive of the Xining Basin, Northwestern China. *Earth and Planetary Science Letters*, *317*, 185-195. https://doi.org/10.1016/j.epsl.2011.11.008

Yang, R., Fang, X., Meng, Q., Zan, J., Zhang, W., Deng, T., Yang, Y., Ruan, X., Yang, L. & Li, B. (2017). Paleomagnetic constraints on the middle Miocene-early Pliocene stratigraphy in the Xining Basin, NE Tibetan Plateau, and the geologic implications. *Geochemistry, Geophysics, Geosystems, 18*(11), 3741-3757. https://doi.org/10.1002/2017GC006945

Yang, R., Yang, Y., Fang, X., Ruan, X., Galy, A., Ye, C., Meng, Q. & Han, W. (2019). Late miocene intensified tectonic uplift and climatic aridification on the Northeastern Tibetan Plateau: evidence from clay mineralogical and geochemical records in the Xining Basin. *Geochemistry, Geophysics, Geosystems, 20*(2), 829-851.

Yang, F., Guo, Z., Zhang, C., Abu Sadat Md, S., He, Z., & Deng, C. (2019). High-resolution Eocene magnetostratigraphy of the Xijigou section: Implications for the infilling process of Xining Basin, northeastern Tibetan Plateau. *Journal of Geophysical Research: Solid Earth, 124*(8), 7588-7603. https://doi.org/10.1029/2019JB017624

Yin, A., Dang, Y. Q., Wang, L. C., Jiang, W. M., Zhou, S. P., Chen, X. H., Gehrels, G. E. & McRivette, M. W. (2008). Cenozoic tectonic evolution of Qaidam basin and its surrounding regions (Part 1): The southern Qilian Shan-Nan Shan thrust belt and northern Qaidam basin. *Geological Society of America Bulletin, 120*(7-8), 813-846. https://doi.org/10.1130/B26180.1

Yuan, D. Y., Ge, W. P., Chen, Z. W., Li, C. Y., Wang, Z. C., Zhang, H. P., Zhang, P. Z., Zheng, D. W., Zheng, W. J., Craddock, W. H., Dayem, K. E., Duvall, A. R., Hough, B. G., Lease, R. O., Champagnac, J. D., Burbank, D. W., Clark, M. K., Farley, K. A., Garzione, C. N., Kirby, E., Molnar, P. & Roe, G. H. (2013). The growth of northeastern

Accepted Article

Tibet and its relevance to large-scale continental geodynamics: A review of recent studies. *Tectonics, 32*(5), 1358-1370. https://doi.org/10.1002/tect.20081

Zhang Y. Q., Ma, Y., Yang, N., Shi, W., & Dong, S. (2003). Cenozoic extensional stress evolution in North China. Journal of Geodynamics, 36(5), 591-613. https://doi.org/10.1016/j.jog.2003.08.001

Zhang, H. P., Craddock, W. H., Lease, R. O., Wang, W. T., Yuan, D. Y., Zhang, P. Z., Molnar, P., Zheng, D. W. & Zheng, W. J. (2012). Magnetostratigraphy of the Neogene Chaka basin and its implications for mountain building processes in the north-eastern Tibetan Plateau. *Basin Research, 24*(1), 31-50. https://doi.org/10.1111/j.1365-2117.2011.00512.x

Zhang, J., & Cunningham, D. (2013). Polyphase transpressional development of a NNE-striking basement-cored anticline in the Xining Basin, northeastern Qinghai–Tibetan Plateau. *Geological Magazine, 150*(4), 626-638. https://doi.org/10.1017/S0016756812000866

Zhang, J., Wang, Y., Zhang, B., & Zhang, Y. (2016). Tectonics of the Xining Basin in NW China and its implications for the evolution of the NE Qinghai-Tibetan Plateau. *Basin Research*, *28*(2), 159-182. https://doi.org/10.1111/bre.12104

Zhang, Y., Dong, S., & Li, J. (2019). Late Paleogene sinistral strike-slip system along east Qinling and in southern North China: Implications for interaction between collision-related block trans-rotation and subduction-related back-arc extension in East China. Tectonophysics, 769, 228181. https://doi.org/10.1016/j.tecto.2019.228181

Zhuang, G., Johnstone, S. A., Hourigan, J., Ritts, B., Robinson, A., & Sobel, E. R. (2018). Understanding the geologic evolution of Northern Tibetan Plateau with multiple thermochronometers. *Gondwana Research, 58*, 195-210. https://doi.org/10.1016/j.gr.2018.02.014

Zuza, A. V., & Yin, A. (2016). Continental deformation accommodated by non-rigid passive bookshelf faulting: An example from the Cenozoic tectonic development of northern Tibet. *Tectonophysics*, 677, 227-240. https://doi.org/10.1016/j.tecto.2016.04.007